FILE: 17C
INITL:

UNIVERSITY OF NEVADA – RENO – NEVADA – 89557

1

Mackay School of Mines
Seismological Laboratory

Telephone (702) 784-4975

15 Feburary, 1985

TS	ACT	INFO
CH		
A CH		
AT C		
TGE		
TGR		
TGT		
TGX		

Air Force Office of Scientific Research
Attn: NP
Bolling Air Force Base
Washington, D.C. 20330

ANNUAL TECHNICAL REPORT

ARPA Order	No. 4397
Program Code	3D60
Grantee:	University of Nevada Regents
Effective Date:	1 Oct 1982
Grant Termination Date:	30 June 1985
Amount of Grant:	$203,692
Grant No.	49620-83-C-0012
Principal Investigators:	Alan S. Ryall (702) 784-4975 Keith F. Priestley (702) 784-4259
Program Manager:	Keith F. Priestley
Short Title of Work:	Attenuation in the western Great Basin

Sponsored by
Advanced Research Projects Agency (DOD)
ARPA Order No. 4397
Monitored by AFOSR Under Grant No. 49620-83-C-0012

SECURITY CLASSIFICATION OF THIS PAGE (When Data Entered)

REPORT DOCUMENTATION PAGE

READ INSTRUCTIONS BEFORE COMPLETING FORM

1. REPORT NUMBER

2. GOVT ACCESSION NO.

3. RECIPIENT'S CATALOG NUMBER

4. TITLE (and Subtitle)

Attenuation in the Western Great Basin

5. TYPE OF REPORT & PERIOD COVERED

Annual Technical Report
10/1/83 - 9/30/84

6. PERFORMING ORG. REPORT NUMBER

7. AUTHOR(s)

Keith Priestley

8. CONTRACT OR GRANT NUMBER(s)

49620-83-C-0012

9. PERFORMING ORGANIZATION NAME AND ADDRESS

Seismological Laboratory, Mackay School of Mines
University of Nevada
Reno, Nevada 89557

10. PROGRAM ELEMENT, PROJECT, TASK AREA & WORK UNIT NUMBERS

61101F

11. CONTROLLING OFFICE NAME AND ADDRESS

Defense Advanced Research Projects Agency
1400 Wilson Blvd.
Arlington, Va. 22209

12. REPORT DATE

2/15/85

13. NUMBER OF PAGES

65

14. MONITORING AGENCY NAME & ADDRESS (if different from Controlling Office)

Air Force Office of Scientific Research
Bolling AFB/Bldg 410
Washington, D.C. 20332

15. SECURITY CLASS. (of this report)

unclassified

15a. DECLASSIFICATION. DOWNGRADING SCHEDULE

16. DISTRIBUTION STATEMENT (of this Report)

Unlimited

17. DISTRIBUTION STATEMENT (of the abstract entered in Block 20, if different from Report)

Unlimited

18. SUPPLEMENTARY NOTES

19. KEY WORDS (Continue on reverse side if necessary and identify by block number)

m_b-M_S, source mechanisms, Mammoth Lakes, Faultless, Hot Creek Valley

20 ABSTRACT (Continue on reverse side if necessary and identify by block number)

Teleseismic P-wave resiudals reveal that beneath the FAULTLESS shot point there is a much smaller high speed anomaly than that observed beneath Pahute Mesa. Ray tracing through the porposed mantle structures in each area result in a shadow zone for European statations for Pahute Mesa shots and little to no effect on energy from FAULTLESS. This suggests that magnitude versus yield curves based on Pahute Mesa explosions are biased, and that the FAULTLESS magnitude versus yield anomaly is a consequence of using those curves.

DD FORM 1 JAN 73 1473 EDITION OF 1 NOV 65 IS OBSOLETE

SECURITY CLASSIFICATION OF THIS PAGE (When Data Entered)

Low frequency estimates of seismic moment of Mammoth Lakes, CA events based on regional surface wave recordings are similar to those using local body wave recordings of the same events. The lack of peaked spectra eliminates one of the proposed dike injection mechanisms. The spectra show no features that suggest mechanisms different from those of "tectonic" earthquakes.

Mammoth Lakes earthquakes discriminate from Nevada Test Site explosions when comparing m_b and M_s.

Observations of peak Wood-Anderson response along travel paths in the Great Basin indicate greater attenuation at regional distances than in southern California by about 0.3 M_L units. Near source M_L estimates are higher that predicted by Richter's attenuation curve, probably due to the poor near source constraint on the curve. Local magnitude for events above $M_L \geq 6$ is seen to saturate at near distances, possibly due to effects of extended source size.

Technical Report Summary

This report is divided into four sections. Section 1 concerns inferences on the crust and upper mantle structure of the Central Nevada Test Site from teleseismic P-wave residuals and its implications for the Faultless magnitude versus yield anomaly. Hot Creek Valley, the site of CNTS, is dominated by a series of nested calderas which range in age from 25 to 35 m.y., 10 to 20 m.y. older than the Silent Canyon caldera at Pahute Mesa. P-wave residuals relative to a Great Basin average show that Hot Creek Valley is relatively fast, suggesting that, as for the case of Silent Canyon at NTS, a high velocity vestage of a root to the Hot Creek calderas exist at depth. Comparing travel-time residuals of explosions in Hot Creek Valley and Silent Canyon relative to an explosion at Yucca Flat indicates slower relative velocities beneath CNTS than at NTS. An explanation for this is that the body under CNTS is probably older and thus has had more time to be assimilated into the surrounding mantle. Ray tracing through the proposed mantle structure beneath Pahute Mesa (Spence, 1974) results in a shadow zone for European stations. A large percentage of the stations reporting magnitudes for the Nevada explosions are from Europe. The effect is much smaller at Hot Creek Valley suggesting that the magnitude vs yield bais might result from using magnitude-yield curves for the larger explosions based on data from Pahute Mesa. We have now obtained the WWSSN data for FAULTLESS, GREELEY, and DUMONT and are plotting amplitude vs distance curves to see if in fact the expected caustic and shadow zone predicted exist in the data.

Section 2 is a manuscript which is in press in the *Journal of Geophysical Research*. In this study, spectra for 24 Mammoth Lakes earthquakes greater than 1×10^{21} dyne-cm, including the M_L 6 event occurring at 1450 UT on May 27, 1980, have been determined. The short-period portion of the spectra (0.5 - 10.0 Hz) have been determined from spectral analysis of the locally recorded strong-motion and broad-band digital data. A relationship has been derived between the Marshall-Basham surface-wave magnitude and seismic moment allowing us to determine the seismic moment directly from time domain amplitude measurements of the surface waves recorded at regional stations. This gives an estimate of the seismic moment independent of that obtained from the S-wave spectra and one based on lower frequencies (0.05 - 0.125 Hz). A comparison of the seismic moments indicate that for any one event, no significant difference in the spectral level exists between the values determined at surface wave frequencies (0.05 to 0.125 Hz) and the S-wave corner frequency (1 to 5 Hz). The events studied, and in particular the 5/27/80--1450 M_L 6 event, do not show peaked spectra predicted from theoretical analysis of the ground motion resulting from a fluid-driven, propagating tensile crack. We have found nothing in the spectra of these events to distinguish them from "tectonic" earthquakes. The absence of a peaked spectrum does not rule out dike injection as the source of these earthquakes, but it does rule out a particular model of magmatic intrusion, namely that of Chouet (1981) and Aki (1984), for a low viscosity fluid.

Section 3 is a draft of a manuscript prepared for submission to the *Geophysical Journal of the Royal Astronomical Society*. In an earlier study, Wyss and Brune (1971) compared short period and long period excitation of events in the California region. They found that events occurring to the north of Bishop,

California indicated higher apparent stress than events along the San Andreas fault. In this study we have looked in detail at the relative excitation of short and long period energy in this region, from aftershocks of the Mammoth Lakes sequence. We have compared the body wave magnitude, mb, and surface wave magnitude, Ms, and find that Mammoth Lakes events discriminate from nuclear explosions occurring at the Nevada Test Site approximately 150 km to the southeast. We have used local strong-motion and broad-band digital recordings to compute the source spectra of 37 earthquakes. For events in common with Archuleta *et al.* (1982) our moments are in agreement. We have developed a moment-surface wave magnitude relationship which allows us to rapidly determine the seismic moment at surface wave periods from time domain amplitude measurements on the long-period seismogram. These determinations of moment in almost all cases agree closely with the moments determined from the spectra. Similar studies in southern California show long-period moments exceeding short-period moments by a factor of 4 to 10. For six events we have compared the magnitude estimates m_b, M_L, and M_s with the spectral amplitude at their appropriate frequencies. Of the four shallow events compared, three, those at 801471857, 801481901, and 801490516, are consistent with the ω^{-2} model. The stress drops of these events are nearly similar but the source dimension of the 801471857 event is nearly twice that of the other two events, which explains its larger moment and greater surface wave excitation. The fourth shallow event had an anomously low surface wave excitation compared to other events and a lower stress drop. The remaining two events, at depths of 8 and 12 kilometers, have similar stress drops and source dimensions to the 801471857 event. However, the 8 km deep event has anomously large surface wave excitation, and the m_b of the deepest event is underestimated by about a factor of five.

In section 4, we have converted 471 seismograms from 103 earthquakes in the vicinity of Mammoth Lakes, California into equivalent Wood-Anderson seismograms and estimated local magnitude M_L following the original definition made by Richter. We found that the distance correction terms given by Richter's attenuation curve yield systematically larger M_L estimates for distances less than 20 km. M_L determined at near distances ($\Delta < 10$ km) using Richter's $\log A_0$ values are as much as 1 magnitude unit greater than M_L determined at regional distances ($\Delta > 50$ km) for the same event. This result is similar to those of recent studies utilizing southern California and northern Baja California earthquakes. Seismograms recorded at greater distances in the Great Basin (100 km $< \Delta <$ 600 km) show more attenuation (about 0.3 magnitude units) than that predicted by Richter's curve. We have determined corrections to the attenuation curve which removes the distance dependence observed for our data. We also find a near source local magnitude saturation for events with $M_L \geq 6.0$ similar to earlier studies with California earthquakes and explained as finite source size effects. Using the revised magnitude scale and seismic moments estimated from spectral analysis we found that our data are well fit by the straight line

$$\log M_o = (1.22 \pm 0.04) M_L + (16.98 \pm 0.15)$$

for $1.5 \leq M_L \leq 6.3$. Comparison of our data to predicted M_o versus M_L values suggest a constant stress drop of approximately 100 bars for events with $M_L < 5.0$ and increasingly greater stress drop for the larger events.

INFERENCES ON THE CRUST AND UPPER MANTLE STRUCTURE OF THE CENTRAL NEVADA TEST SITE FROM TELESEISMIC P-WAVE RESIDUALS AND ITS IMPLICATIONS FOR THE *FAULTLESS* MAGNITUDE VERSUS YIELD ANOMALY

David E. Chavez and Keith F. Priestley

The underground nuclear explosion FAULTLESS was detonated at the Central Nevada Test Site (CNTS) in Hot Creek Valley, Nevada, approximately 150 km north-northwest of the Nevada Test Site (NTS). The ISC body wave magnitude, m_b, of 6.3 is more than 0.3 units (a factor of two in amplitude) greater than that predicted from emperical magnitude-yield curves for NTS explosions, given the announced maximum yield of 1200 kilotons. CNTS is physiographically very similar to Pahute Mesa (NTS), so in view of the close proximity of th two test sites it might be expected that the magnitude-yield curves for NTS would also apply to CNTS.

Spence (1974) used travel-time residuals for NTS explosions recorded at teleseismic distances to infer the presence of a high velocity structure in the mantle beneath the 14 m.y. old Silent Canyon caldera at Pahute Mesa. He attributed the higher velocities to material depleted of its partial melt component by differentiation and by eruption through the caldera. Later studies have confirmed his initial observations. In order to see if any anomalous structures of a similar nature exist beneath CNTS which could produce the discrepancy in observed m_b for FAULTLESS, we have examined teleseismic P-wave residuals as computed from a seven-station temporary network in Hot Creek Valley.

Figure 1 is a map giving the generalized geology, station locations, and the FAULTLESS shot point. As seen from the map, the area around Hot Creek Valley is dominated by a series of nested calderas which range in age from 25 to 35 m.y.; these calderas are 10 to 20 m.y. older than Silent Canyon caldera at Pahute Mesa. However, Hot Creek Valley is also the site of very recent volcanism. For instance, much of the Quaternary basalt shown on the map is sufficiently young that no erosion is evident.

We first searched for local lateral variations in structure by computing teleseismic P-wave residuals relative to the average residual across the network for each event. In Figure 2 we present maps which show relative residual as a function of azimuth for each CNTS station. Each station location is indicated by a circle whose radius is 0.5 second. The circumference represents a zero residual, and lines drawn from the circle are scaled according to the size of the residual. Lines inside the circle are negative residuals (early arrivals) and lines outside the circle are positive residuals (late arrivals). The azimuth of each line corresponds to the azimuth of approach of the wavefront.

Beneath each map is an array diagram, which is a plot of mislocation vectors, i.e., the vector difference between the expected location vector (azimuth of approach and slowness) and that which is measured by fitting a plane wave to the data. The existence of mislocation vectors is due to differences between the earth model used to determine the expected location vector and the real earth. Mislocation vectors of differing magnitude and/or direction are indicative of lateral heterogeneities between the source and receiver.

The first pair of figures are for uncorrected data. The large positive residuals at CNBC are due to approximately 1 km of sediments. In the second pair, the data have been corrected for surface geology which results in a systematic mislocation to the southwest as evident from the array diagram. This mislocation can be removed by correcting the data for a Moho striking $N\ 43^{\circ}\ E$ with 3° dip. This interpretation is consistent with observations of Pn velocity across the network and with the regional Bouguer gravity anomaly.

In Figure 3, we give x-y plots of residual versus azimuth for the data which have been corrected for the sediments and inferred Moho dip. As seen, much of each observed residual is removed by these corrections. The late arrivals at CNBC are probably due to insufficient sediment correction. Two stations, CNPS and CNEC, continue to display an anomalous pattern in that for events arriving from the northwest they both show a large variation in residual. For emphasis, we have isolated the plots for these two stations in a box in the lower right-hand corner of the figure. As shown by the two plots in the extreme lower right, the residuals at CNPS and CNEC show a very definite dependence on angle of incidence. The anomaly at CNPS, which is also somewhat evident at CNHC, has not yet been interpreted. We believe that the anomaly at CNEC is related to its proximity to the Lunar Craters volcanic field.

We have used a simple geometrical argument to qualitativly estimate the position of the suspected body responsible for the CNEC anomaly. Figure 4 is a vie v along a line passing through stations CNHM and CNEC. The stippled regions are what is sampled by our teleseismic data, where the heavy shading indicates normal arrivals, and the lighter indicates the largest possible area causing the delay at CNEC. We observe arrivals as late as 0.3 sec, comprable to that reported by Steeples and Iyer (1976) for stations in Long Valley caldera which they attributed to anomalously hot rock. Subsequent studies in Long Valley have revealed areas of S-wave shadowing associated with the delay that have been interpreted as evidence for the presence of magma (Sanders, 1984). In view of the young volcanics present in Lunar Craters it is not unreasonable to conclude that a similar situation exits here.

Residuals relative to event average, such as we have done, will not reveal any regional velocity anomalies, so we have also computed residuals relative to a regional event average using many stations throughout the Great Basin. The results are shown in Figure 5a. We see that Hot Creek Valley is relatively fast, suggesting that, as in Silent Canyon, a high velocity vestige of a root to the Hot Creek calderas exits at depth. Comparing travel-time residuals the explosion in Hot Creek Valley and Silent Canyon relative to an explosion at Yucca Flat (Figure 5b) indicates slower relative velocities beneath CNTS than at NTS. An explanation for this is that the body under CNTS is probably older and thus has had more time to be assimilated into the surrounding mantle.

In view of these observations, we felt that ray tracing may shed light on the m_b versus yield discrepancy between Hot Creek Valley and Pahute Mesa. Shown in Figure 6 are ray paths through the postulated high speed bodies beneath both regions. The diagrams indicate that for Pahute Mesa events there is a caustic near 50 degrees and defocussing at greater distances. The model for Hot Creek

Valley has only a limited effect.

Most m_b measurements of Nevada nuclear explosions are made from European stations which lie in the Pahute Mesa shadow zone. Consequently, we suspect that m_b vs yield averages based on Pahute Mesa events may be biased and thus when applied to FAULTLESS give a too high yield. For the remainder of the contract period we will examine WWSSN recordings of FAULTLESS, DUMONT, and GREELEY to see if any such shadowing effects can be observed.

References cited

Sanders, C.O., 1984, Location and configuration of magma bodies beneath Long Valley, California, determined from anomalous earthquake signals, *J. Geophy. Res.*, vol. 89, pp 8287-8302.

Spence, W., 1974, P-wave residual differences and inferences on an upper mantle source for the Silent Canyon volcanic centre, southern Great Basin, Nevada, *Geophy. J. R. Astr. Soc.*, vol. 38, pp 505-523.

Steeples, D.W., and H.M. Iyer, 1976, Low-velocity zone under Long Valley as determined from teleseismic events, *J. Geophy. Res.*, vol. 81, pp 849-860.

Stewart, J.H., 1980, Geology of Nevada, *Nevada Bureau of Mines and Geology, Special Publication 4.*

Stewart, J.H., and J.E. Carlson, 1977, Million scale geologic map of Nevada, *Nevada Bureau of Mines and Geology, Map 57.*

Figure captions

Figure 1. Generalized geologic map of the Hot Creek Valley, Nevada area including station locations and the FAULTLESS shot point. Geology from Stewart and Carlson (1977), caldera boundaries from Stewart (1980).

Figure 2. Maps of travel time residuals versus azimuth and array diagrams (format described in the text).

Figure 3. Plots of resiudal versus azimuth for all stations after corrections for surface geology and inferred Moho dip have been applied. The data outlined in the lower right corner are for stations CNPS and CNEC and include plots of residual versus angle of incidence.

Figure 4. Sectional view along a line passing through stations CNHM and CNEC. Shading described in the text.

Figure 5. a) Map of residual relative to event average which includes data from several Great Basin seismic stations, as well as those shown on the map. b) Map of residuals for FAULTLESS and GREELEY relative to DUMONT using ISC

arrival times.

Figure 6. a) Ray paths through the high speed body under Pahute Mesa as postulated by Spence (1974). b) Ray paths through the high speed body under Hot Creek Valley as suggested by our data. Figure 6. a)

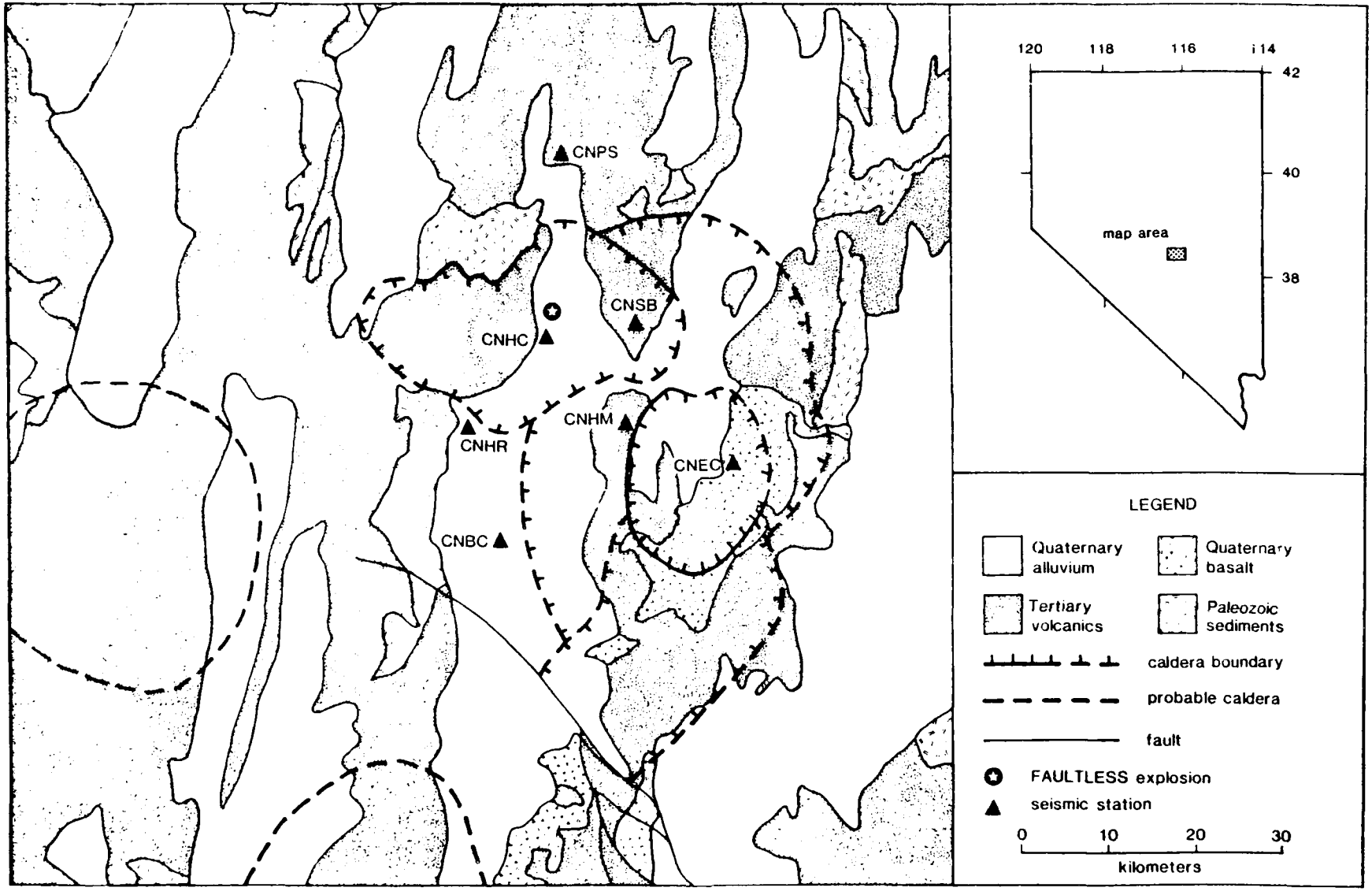
CNPS
CNSB
CNHC
CNHM
CNHR
CNEC
CNBC
120
118
116
114
42
40
38
map area
LEGEND
Quaternary alluvium
Quaternary basalt
Tertiary volcanics
Paleozoic sediments
caldera boundary
probable caldera
fault
FAULTLESS explosion
seismic station
0
10
20
30
kilometers

FIGURE 1

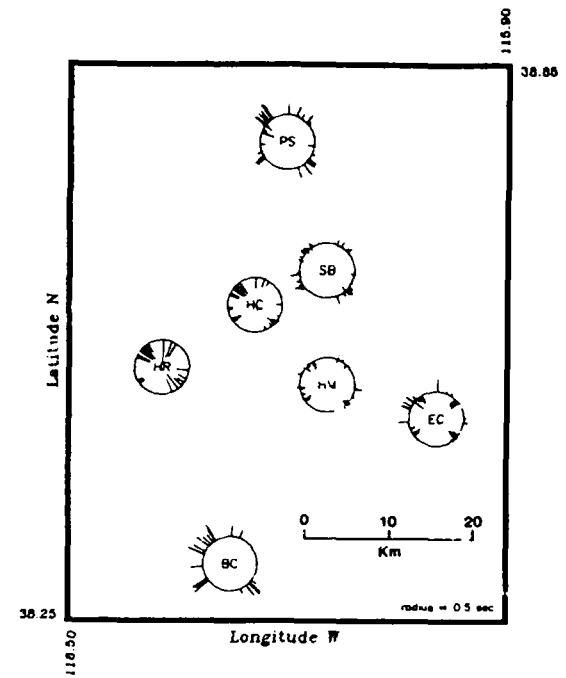

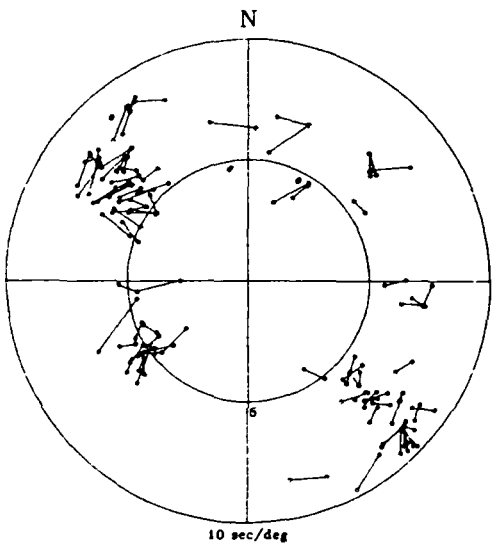

O Expected ● Observed

Uncorrected data

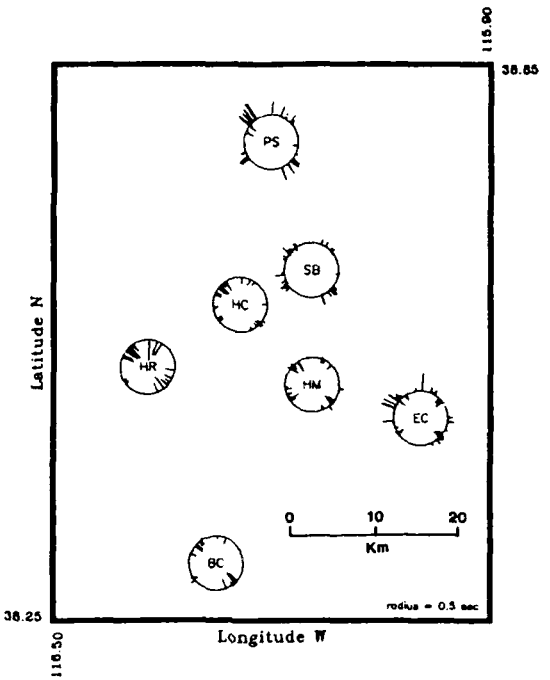

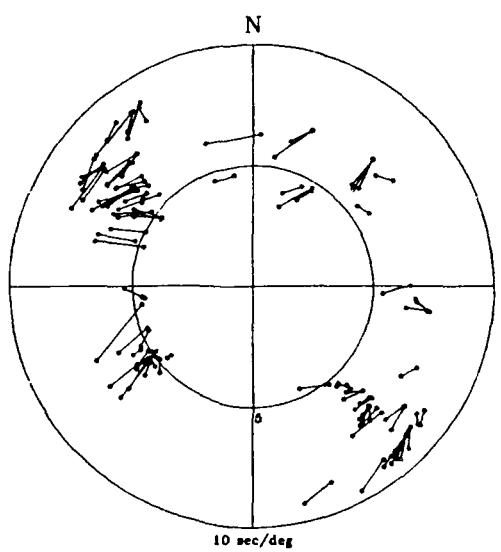

O Expected ● Observed

Sediment corrected

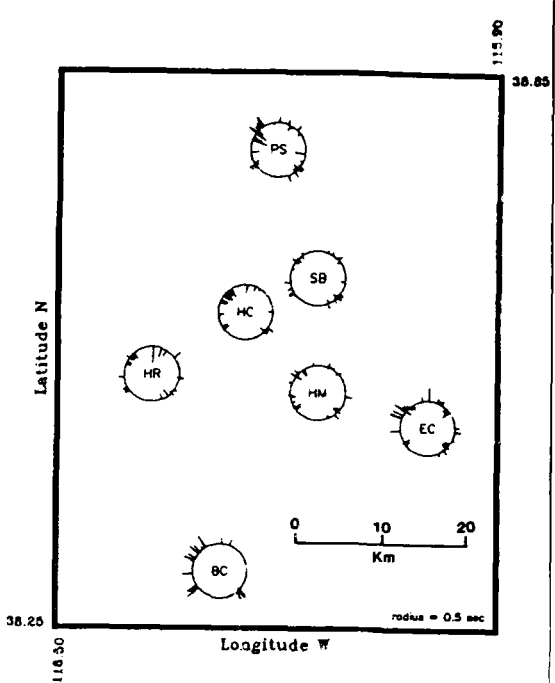

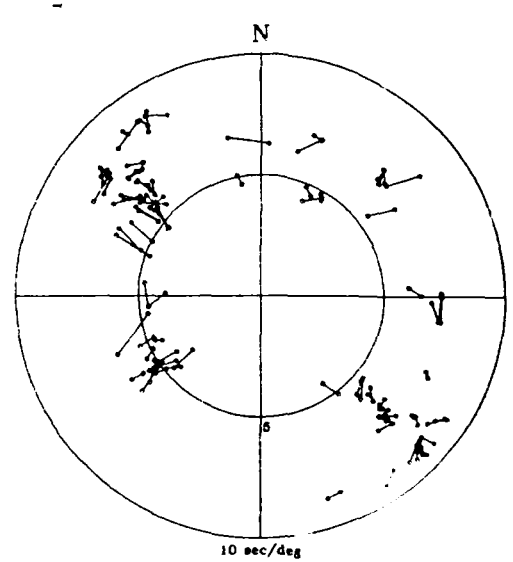

O Expected ● Observed

Moho dip corrected

FIGURE 2

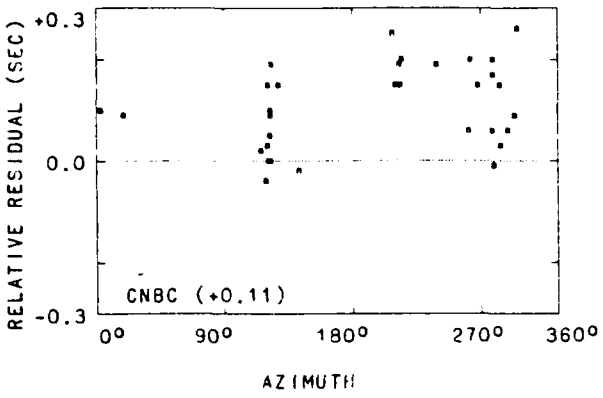
RELATIVE RESIDUAL (SEC)
+0.3
0.0
-0.3
CNBC (+0.11)
0°
90°
180°
270°
360°
AZIMUTH

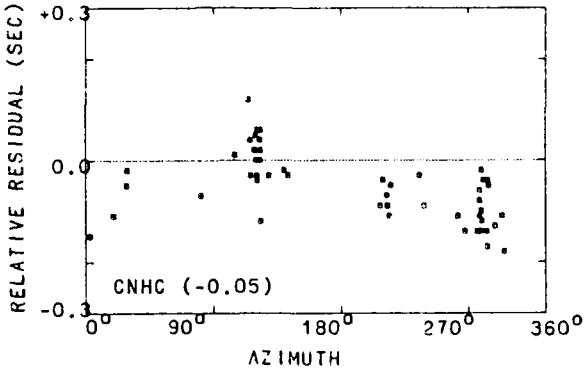
RELATIVE RESIDUAL (SEC)
+0.3
0.0
-0.3
CNHC (-0.05)
0°
90°
180°
270°
360°
AZIMUTH

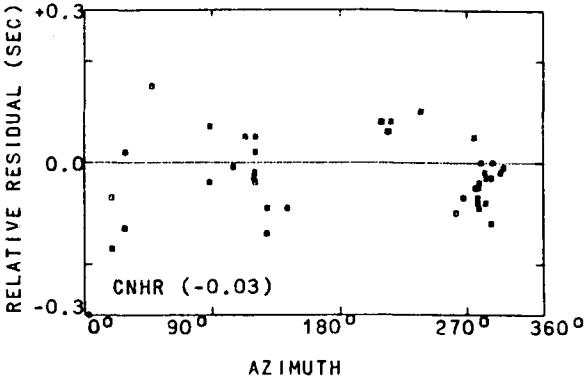
RELATIVE RESIDUAL (SEC)
+0.3
0.0
-0.3
CNHR (-0.03)
0°
90°
180°
270°
360°
AZIMUTH

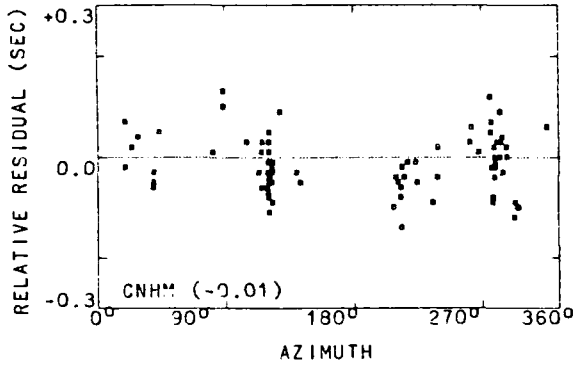
RELATIVE RESIDUAL (SEC)
+0.3
0.0
-0.3
CNHM (-0.01)
0°
90°
180°
270°
360°
AZIMUTH

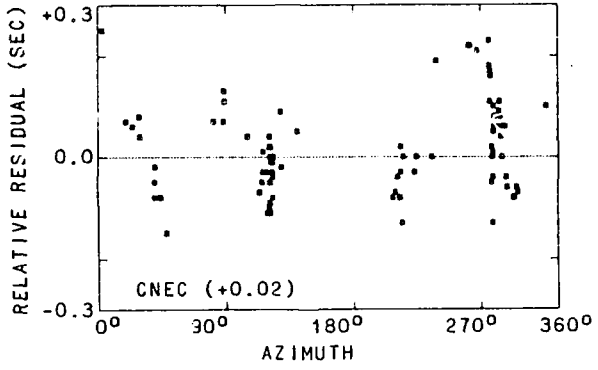
RELATIVE RESIDUAL (SEC)
+0.3
0.0
-0.3
CNEC (+0.02)
0°
30°
180°
270°
360°
AZIMUTH

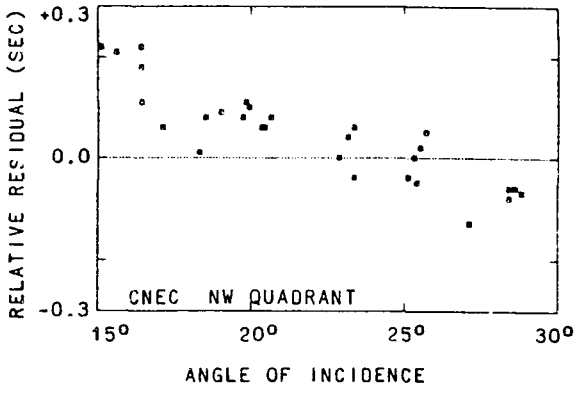
RELATIVE RESIDUAL (SEC)
+0.3
0.0
-0.3
CNEC NW QUADRANT
15°
20°
25°
30°
ANGLE OF INCIDENCE

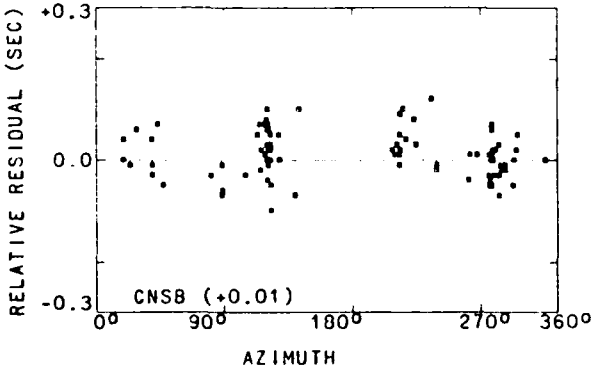
RELATIVE RESIDUAL (SEC)
+0.3
0.0
-0.3
CNSB (+0.01)
0°
90°
180°
270°
360°
AZIMUTH

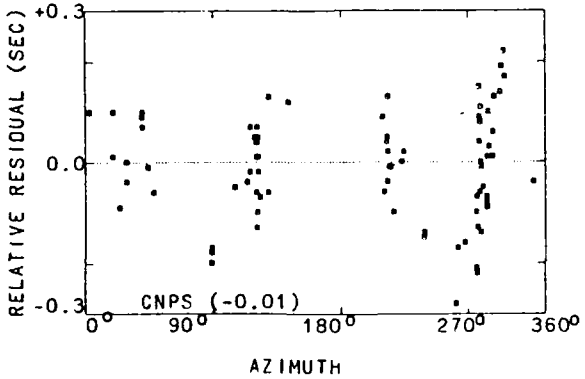
RELATIVE RESIDUAL (SEC)
+0.3
0.0
-0.3
CNPS (-0.01)
0°
90°
180°
270°
360°
AZIMUTH

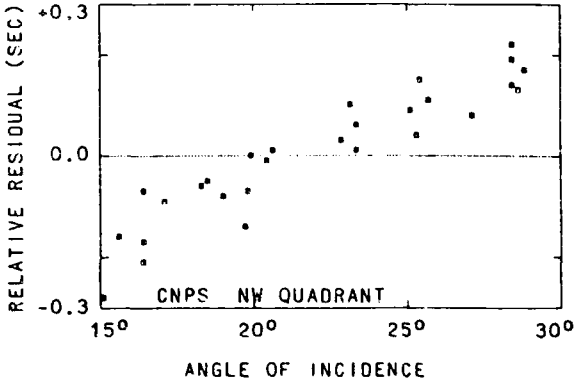
RELATIVE RESIDUAL (SEC)
+0.3
0.0
-0.3
CNPS NW QUADRANT
15°
20°
25°
30°
ANGLE OF INCIDENCE

FIGURE 3

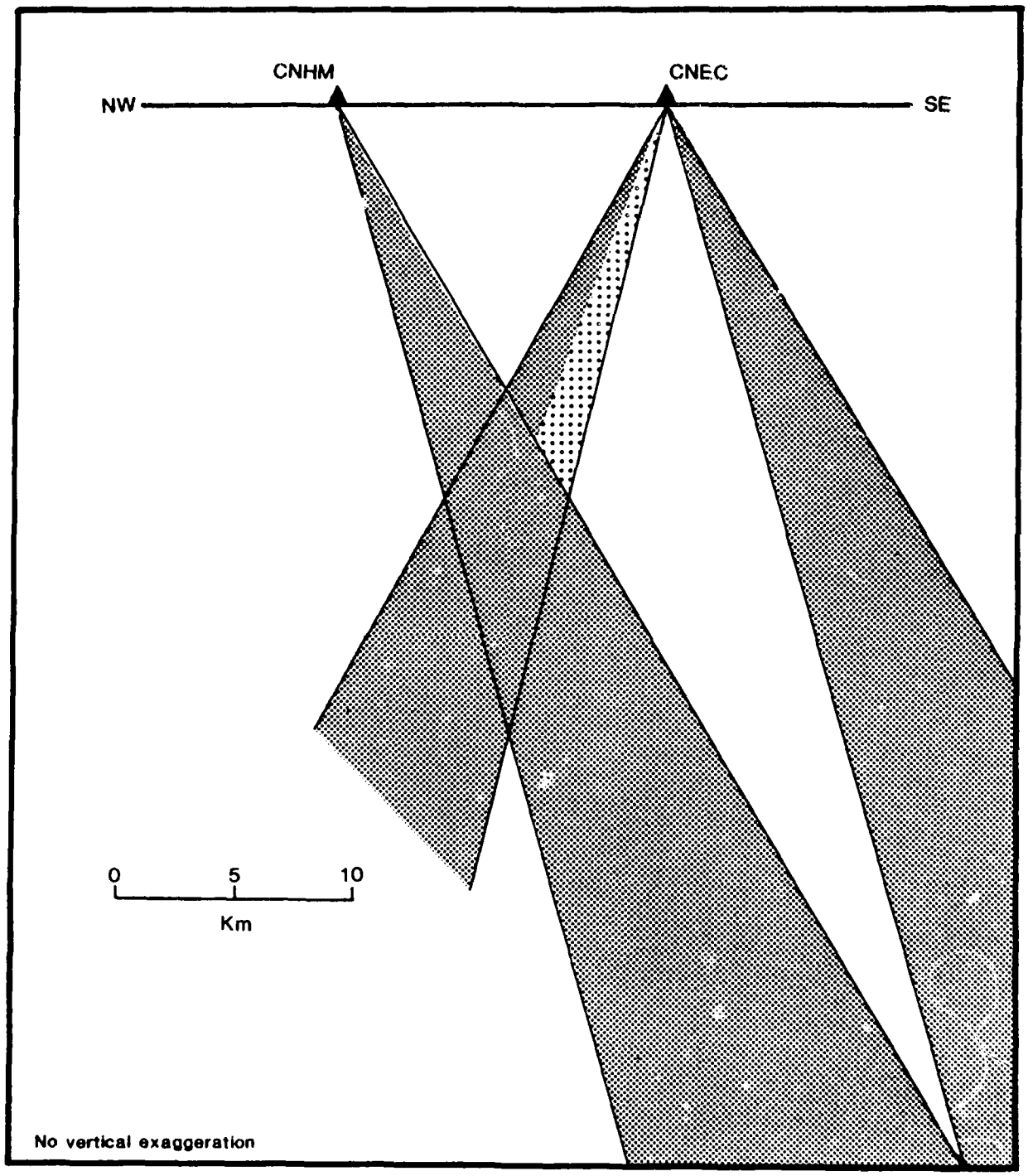

FIGURE 4

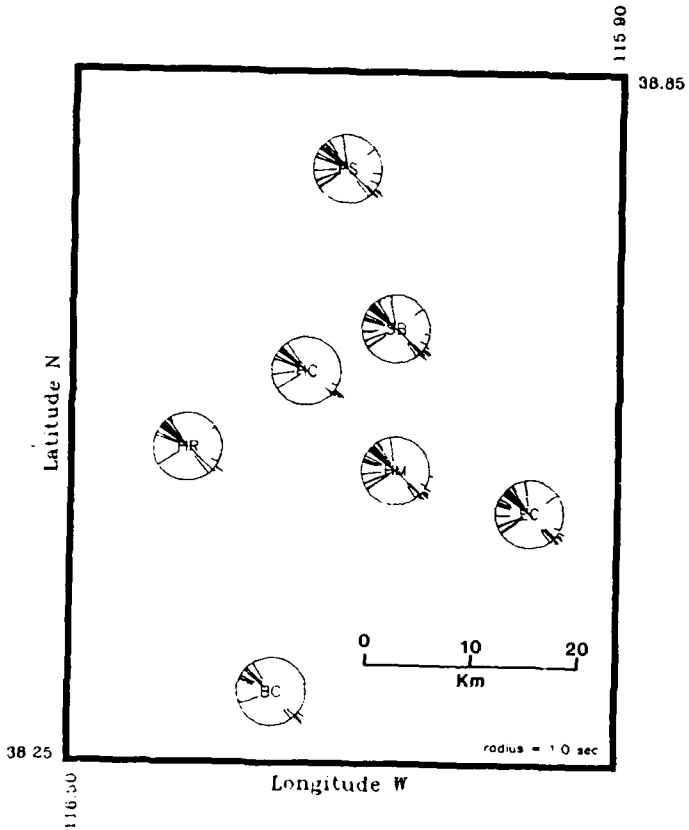

CNTS residuals relative to regional average

(a)

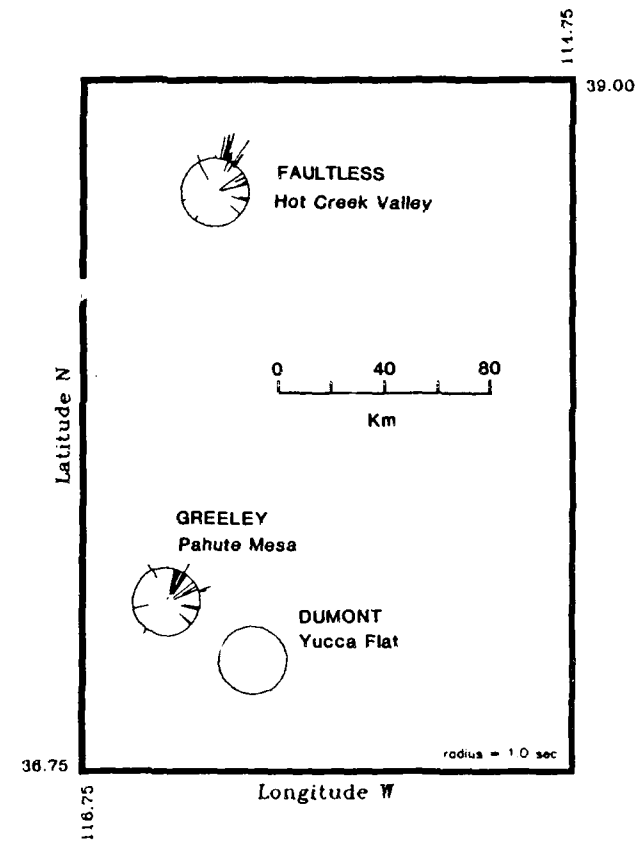

Explosion residuals relative to DUMONT

(b)

FIGURE 5

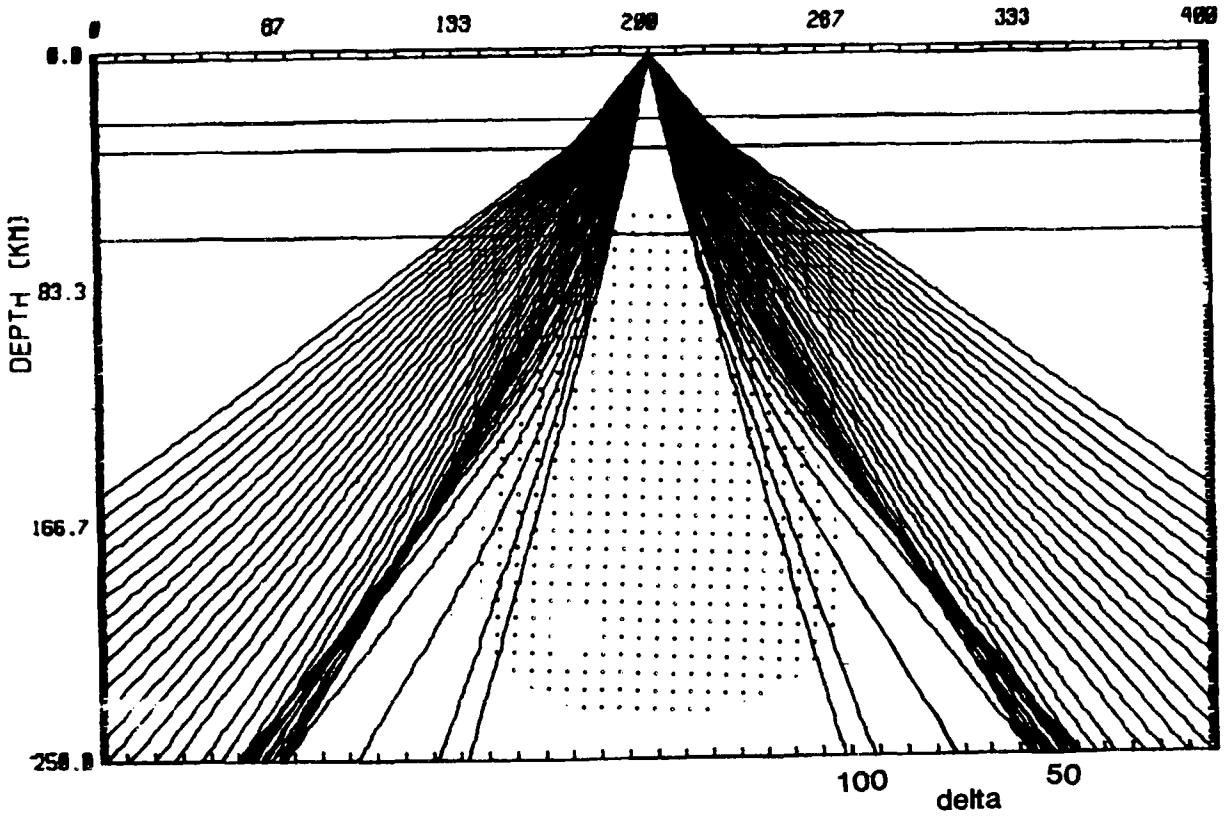

(a) Pahute Mesa

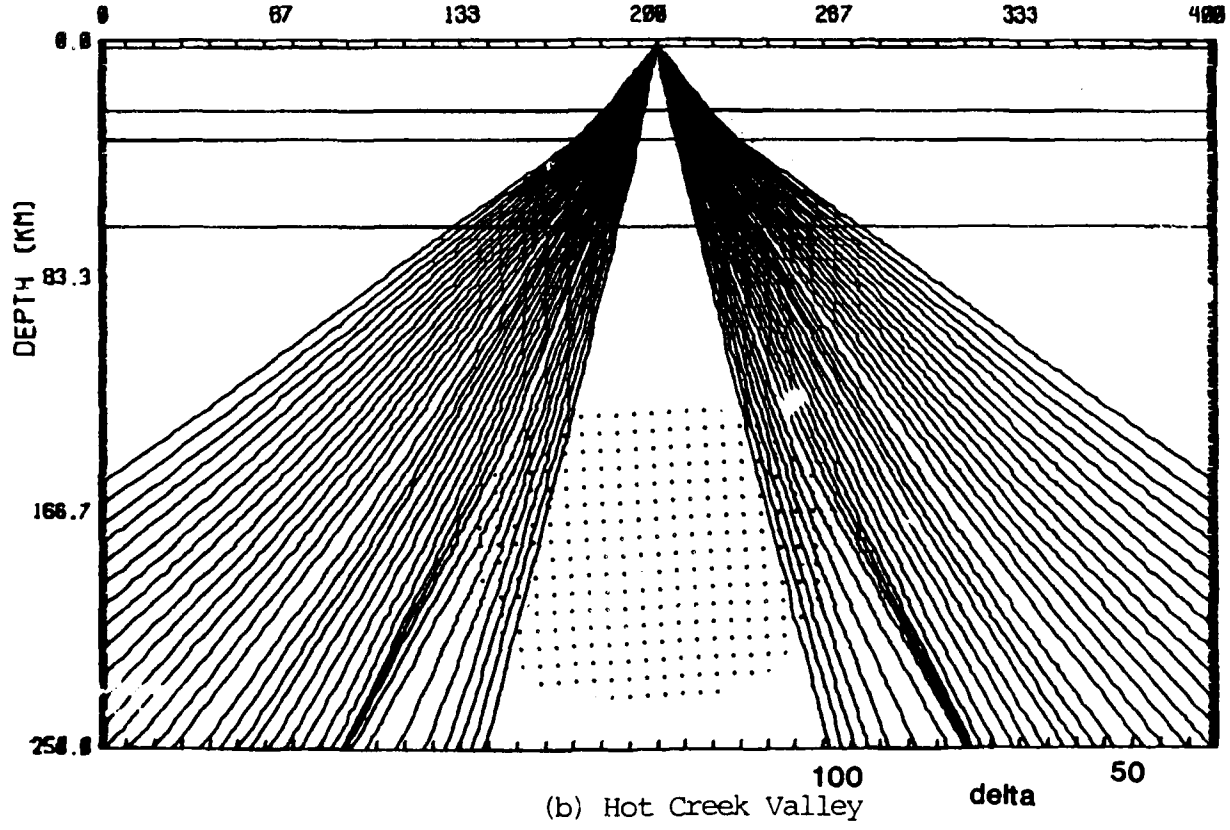

(b) Hot Creek Valley

FIGURE 6

SURFACE WAVE EXCITATION AND SOURCE MECHANISMS OF THE MAMMOTH LAKES EARTHQUAKE SEQUENCE

Keith F. Priestley

Seismological Laboratory, University of Nevada, Reno, NV 89557

James N. Brune, and John C. Anderson

Institute of Geophysics and Planetary Physics
Scripps Institution of Oceanography
University of California, San Diego
La Jolla, California 92093

ABSTRACT

Spectral amplitudes for 24 events of the Mammoth Lakes earthquake sequence have been determined for the frequency range 0.1 to 10.0 Hz. The M_L 6 earthquake that occurred at 1450 UT on May 27, 1980 is of particular interest because of the controversy surrounding its mechanism. A comparison of spectral levels determined from analysis of locally recorded strong-motion and broad-band digital data, and spectral levels from regionally recorded surface waves extrapolated back to the source yield consistent results indicating flat spectra in the band 0.1 - 1.0 Hz. The specta observed in this study do not show pronounced spectral peaks predicted by theoretical studies of gound motion due to the jerky extension of a fluid driven tensile crack containing a low viscosity fluid. We have found nothing in the spectra of the M_L 6 event that occurred at 1450 UT, on May 27, 1980 nor in the spectra of the aftershocks to distinguish them from spectra of "tectonic" earthquakes. However, the spectra themselves do not distinguish between various possible explanations for the non-double couple source mechanism observed in moment tensor inversion and first motion data for the largest events of the Mammoth Lakes earthquake sequence.

Introduction

The Mammoth Lakes earthquakes are located at the intersection of the Sierra Nevada frontal fault system and the Long Valley caldera. The caldera was formed 0.7 million years ago by collapse and subsidence associated with the eruption of the Bishop tuff (Bailey *et al.*, 1976), and volcanism has continued on a reduced scale into the Holocene. The dominant fault in the area south of the caldera is the Hilton Creek fault along which several hundred meters of pure normal fault displacement has occurred since the formation of the caldera (Bailey *et al.*, 1976). Extension of the Hilton Creek fault into the caldera appears to have occurred as recently as 0.3 million years ago, possibly indicating that the caldera had cooled sufficiently by that time to support stresses large enough to generate earthquakes.

The Mammoth Lakes earthquake sequence clearly began with an M_L 5.8 event on October 4, 1978, located beneath the Wheeler Crest 30 km northwest of Bishop, California. Following this event activity gradually spread to the north and west. The main energy release, which began on May 25, 1980, was preceded for over a year by M_L 3.5–4.5 earthquake swarms in the region of the M_L 6 events. These swarms generally clustered near the southern boundary of the caldera, and migrated eastward towards the eventual epicenter of the first M_L 6 event (Cramer and Toppozada, 1980). The main episode of strain release commenced with an M_L 6.1 (all local magnitude estimates for the main events are from Uhrhammer and Ferguson, 1980) event at 1633 UT on May 25 (hereafter referred to as 5/25/80--1633), and was followed by a second M_L 6.0 event at 1649 UT. These initial events occurred along an east-west trend near the southern boundary of the caldera. Seismicity then migrated southward from the caldera boundary. Cramer and Toppozada (1980) note that no events at the magnitude 5 level occurred south of the southern boundary of the caldera until after the M_L 6.1 event at 1944 UT, which occurred six to seven kilometers south of the first M_L 6 event. The last of the large events (M_L 6.2) occurred about nine kilometers south of the 1944 event, at 1450 UT on May 27 (hereafter referred to as 5/27/80--1450). Lide and Ryall (1984) have found that in the two months following the main events, aftershocks and continuing swarms occurred along the southern boundary of the caldera, and along several NNE-SSW trends nearly orthogonal to the caldera boundary. The first and second M_L 6 events occurred along the first of these trends, and the first, third and last of the M_L 6 events occurred along the latter trend. The epicenters of nearly all of the aftershocks and all of the M_L 6 events are well to the west of the projection of the Hilton Creek fault at depth indicating that this is not the causative fault for the earthquake sequence.

Considerable controversy has arisen regarding the source mechanisms of the larger events of the Mammoth Lakes sequence. Focal mechanisms derived from local and regional first motion data indicate strike-slip motion with a NE-SW T-axis and NW-SE P-axis (Cramer and Toppozada, 1980; Ryall and Ryall, 1980). This implies right-lateral motion on east-west trending faults, or left-lateral motion on north-south trending faults. Unconstrained moment-tensor inversion of long-period teleseismic body and surface-wave data result in a large, non-double-couple component for the first and last of the M_L 6 events, and the inversion of the teleseismic waveform data plus teleseismic first motion data indicate mechanisms for the first, third and fourth of the M_L 6 events which differ significantly from strike-slip (Given *et al.*, 1982; Barker and Langston, 1983).

The observed non-double couple mechanism may arise in a number of ways. Given *et al.* (1982) have constrained the moment tensor to be a double - couple and interpreted the results in terms of left-lateral oblique slip on NNE trending planes dipping eastward. They suggest that the discrepancy between the regional and teleseismic mechanisms could arise from either structural effects which distort the teleseismically observed radiation pattern, or complex rupture during the event. Distortion of the outgoing rays may result from complex structure beneath the Long Valley caldera, for example the presence of magma chambers which were first proposed by Hill (1976). Similar anomalies in focal mechanisms have been reported for mid-oceanic ridge earthquakes, and these have been attributed to defocusing of the ray paths due to magma beneath the rise crest (Solomon and Julian, 1974). Wallace (1984) and Lide and Ryall (1984) have interpreted the non-double couple mechanism as arising from a multiple source. Reversal of polarity observed on short-period and long-period instruments at the same site (Wallace *et al.*, 1982) suggest a complex source time function with the short period arrivals representing the failure of an asperity

(possibly with a strike slip mechanism, and the long-period arrivals due to the overall response of the faulting episode. Similar non-double couple mechanisms for events in Greece, have been shown to be the result of events with rupture on multiple planes (D. MacKenzie, personal communications, 1984).

On the other hand, Julian (1983) has suggested that the results of inverting the surface wave and long-period body wave data, and taking the regional and teleseismic first motion data as a whole, are better fit by a compensated linear vector dipole (CLVD) mechanism (Knopoff and Randall, 1970), than they are by a double-couple mechanism. Julian has noted that the CLVD mechansm is consistent with all but four and two of the first motion data, respectively, for the 5/25/80--1633 and 5/27/80--1450 M_L6 events, as opposed to 32 and 16 inconsistent data for the double couple mechanism, and has suggested that the 5/25/80--1633 and 5/27/80--1450 events are due to injection of a fluid into an expanding crack, i.e., dike formation. Aki (1984), utilizing the calculations of Chouet (1981), has suggested that the non-double couple mechanism results from the rapid opening of a channel between two pre-existing cracks filled with magma.

In this study we compare spectral amplitudes of 24 Mammoth Lakes earthquakes ranging in magnitude from M_L 3.5 to M_L 6.2, over the frequency band ≈ 0.05 - 20 Hz. Spectral amplitudes from approximately 0.5 to 20 Hz are derived from spectral analysis of locally recorded body-wave data. Spectral amplitudes from approximately 0.05 to 0.125 Hz are derived from analysis of regionally recorded surface wave data. The wide bandwidth of the spectral amplitude measurements allows us to compare the observed spectral shapes with theoretical spectral shapes for ground motion resulting from "tectonic" earthquakes and ground motion predicted for a propagating tensile crack.

Data

This study is based on seismograms of the Mammoth Lakes earthquakes recorded on the seismic stations shown in Figure 1. The events, shown as dots, comprise only a small fraction of the total number of events which have occurred in the Mammoth Lakes area since October, 1978. Locations after May 27, 1980 are largely from Lide (written communication, 1984). Locations for some of the earlier events are from the University of Nevada or University of California at Berkeley bulletins. The events selected for analysis were those recorded on at least one local strong-motion or digital seismograph and one long-period regional seismograph. The SMA-1 strong-motion accelerographs, shown as triangles in Figure 1, were installed by the California Division of Mines and Geology (Turpin, 1980), or by the University of Southern California (USC) (Moslem *et al*, 1983). We also used shear wave spectra supplied by Ralph Archuleta from data recorded by the U.S. Geological Survey. Digital stations, shown by squares in Figure 1 and described by Archuleta *et al*. (1982), consist of either force-balance accelerometer or velocity transducers and Sprengnether DR-100 recorders. For events along the southern boundary of the caldera, the SMA-1 and digital seismographs cover a large fraction of the focal sphere compared with many previous studies of a similar nature. The radiation pattern of events south of the caldera are not as well sampled.

The inset map in Figure 1 shows the locations of the regional long-period stations from which seismograms were used to determine surface wave magnitude. These stations completely surround the Mammoth Lakes region and, are all WWSSN stations, with the exception of the California Institute of Technology (CIT) station at Pasadena (PAS).

Analysis

Determination of Body-Wave Moment: Displacement amplitude spectra were computed by Fourier transforming the S-wave arrival on the strong-motion accelerograms, and then dividing the acceleration spectra by ω^{-2} to give the displacement spectra. The time window was chosen to be long enough to include the entire S-wave arrival, but short enough to minimize the inclusion of surface-wave energy. The spectra have been normalized to a distance of 10 km. Since the precise locations of the foci of the events are not known, we have not used the epicenter and seismograph coordinates to determine the distance, but have estimated the epicentral distance R from the S-P times assuming an avarage S-wave velocity of 3.4 $km\ s^{-1}$ and an average P-wave velocity of 5.8 $km\ s^{-1}$. In addition, we have not rotated the data into transverse and radial components, but have computed the spectra for both horizontal components and computed the vector sum of these two values.

The spectra were interpreted in terms of a flat, low-frequency asymptote Ω_0, a high frequency ω^{-2} falloff, and the corner frequency f_c at which the two trends intersect. The far-field spectral parameters were then related to the source parameter seismic moment M_0 using the relationship given by Brune (1970, 1971)

$$M_0 = \frac{4\pi\rho\beta^3\Omega_0 R}{kR_{\vartheta\varphi}} \tag{1}$$

where ρ is the density ($\rho = 2.8\ g\ cm^{-3}$), β is the shear-wave velocity ($\beta = 3.5\ km\ s^{-1}$), $R_{\vartheta\varphi}$ is the RMS average of the radiation pattern (taken here as 0.6), and k is a correction factor for the amplification of SH waves at the free surface (taken as 2). The correction of the amplitude of the S-wave on being reflected at the free surface assumes that the waves are horizontally polarized (SH). Since we have not rotated the data into transverse and radial components, the data are in general some mixture of SH and SV motion. Abe (1974) discusses experimental studies of amplification on reflection and concludes that using $k = 2$ applies approximately to SH-wave signals containing some SV motion. Helmberger and Malone (1975) discuss problems due to multiple arrivals caused by reflections in deducing source parameters from S-waves recorded at epicentral distances much greater than the source depth. The station-source configuration shown in Figure 1 indicates that this should not be a problem in this study.

A source of error inherent in the estimate of Ω_0 and consequently in the estimates of M_0 comes from the assumption of a single, average correction for radiation pattern. If sufficient instruments were available, or if the source parameters including direction and velocity of rupture were known, this source of error could be reduced. A value of 0.6 was used for $R_{\vartheta\varphi}$ (Thatcher and Hanks, 1973). At some azimuths, the amplitude could be 1.67 times larger than the amplitude determined assuming this correction, while near a node in the radiation pattern the amplitude could be quite small. Furthermore, if the source dimension is comparable to the wavelength involved, source propagation might distort the radiation pattern by focusing or defocusing energy, thereby changing the apparent corner frequency for different directions and possibly reducing the calculated moment.

No Q correction was made in determining the spectra. Archuleta *et al.* (1982) found that whole-path Q had a small effect on the measurement of Ω_0 for Mammoth Lakes events.

Determination of Surface Wave Moment: Tucker and Brune (1977) determined the seismic moment of seven aftershocks of the San Fernando earthquake from the surface wave spectra. This gave an estimate of seismic moment independent of that obtained from S-wave spectra and one based on lower frequencies (0.03 - 0.10 Hz in their case). They made a careful estimate of the errors involved in estimating the seismic moment from the surface wave spectra. The errors included procedural errors, path structure and attenuation, lateral refraction (multipathing), source finiteness, and uncertainties in fault parameters (depth, dip, strike, and slip vector) in correcting for radiation pattern. They concluded that these effects could lead to a maximum error in the final result of no more than a factor of 4.

In this study we also determined the seismic moment from surface waves for comparison with seismic moments determined from the S-wave spectra. However, we used a different procedure which allowed us to determine the seismic moment from a large number of events without the time-consuming digitization of the surface wave seismograms.

Surface wave magnitude (M_S) defined by the formula (Marshall and Basham. 1972)

$$M_S = Log\ A + B'(\Delta) + P(T) \qquad (2)$$

was determined from seismograms of long-period seismograph stations, primarily in the western United States. In equation (2), A is one-half the peak-to-peak ground amplitude of the maximum amplitude Rayleigh wave with period T at distance Δ. $B'(\Delta)$ corrects for average attenuation, scattering, geometrical spreading and refraction; and $P(T)$ is a correction factor for dispersion and allows measurement of the surface-wave amplitude at any period. Marshall and Basham (1972) have tabulated $P(T)$ for continental North America for periods ranging from 10 to 40 seconds. In some cases the maximum surface-wave amplitude observed for the Mammoth Lakes earthquakes was in the 8 to 10 second range. Since $P(T)$ is a smoothly varying function, we have extrapolated $P(T)$ to eight seconds period. The surface wave-magnitudes for the Mammoth Lakes events studied here are tabulated in Table 1.

The surface-wave moment is linearly related to the surface wave amplitude, and thus to the surface wave magnitude. We have determined a relationship between the surface-wave magnitude and the seismic moment in the following manner. Surface wave synthetics were generated by a computer routine (written by Guy Masters) for an earthquake with $M_o = 10^{21}$ dyne-cm at a number of regional seismographs from which data were used to determine the surface-wave magnitudes. From the synthetic surface wave seismograms, we determined the surface wave magnitude in the same manner as discussed above for the Mammoth Lakes earthquakes, and thus determined a relationship between the surface wave magnitude and seismic moment.

Factors affecting the calculation of the synthetic surface wave seismograms are the earth velocity and attenuation structure and the fault parameters of the individual earthquakes. Since the events are located at the western edge of the Great Basin, while most of the seismograph stations are located in western North America, we have used the velocity structure determined for the Great Basin from surface wave dispersion measurements (Priestley and Brune, 1978). The attenuation structure for the Great Basin by Patton and Taylor (1984) was used, with a slight lowering of Q_β from that of Patton and Taylor in the surficial layer. Since we do not have fault-plane solutions nor do we know the focal depth for the majority of events we have studied, we determined an average relationship for the Mammoth Lakes area in the following manner. Vetter and Ryall (1983) have

determined fault plane solutions for a large number of events in the Mammoth Lakes area, and found that the mechanisms can generally be divided into two groups. The first group consists of earthquakes with strike-slip mechanisms (average plane of strike N14°E, dip 80°ESE, slip N16°E or strike N73°W, dip 80°SSW, slip N76°E) which are most commonly at depths less than 9 km. The second group consists of earthquakes with oblique or normal mechanisms (average planes of strike N03°E, dip 64°E, slip N40°E or strike N50°W, dip 38°SW, and slip N86°W)usually at depths greater than 9 km. Synthetic surface wave seismograms were calculated for both mechanisms for 2, 5, 8, 11 and 14 km depth. Surface-wave magnitudes were determined from the 10 records at each station and an average conversion factor determined for both focal mechanisms and all focal depths. The resulting relationship between surface wave magnitude M_S and seismic moment M_0 for the Mammoth Lakes area is given by the equation

$$\log M_0 = M_S + 19.40(\pm 0.06) . \qquad (3)$$

To verify the validity of our moment-surface wave magnitude relationship, we can compare equation (3) with other moment magnitude relations established for the western United States. Wyss and Brune (1968) originally established a moment-local magnitude relationship for events less than magnitude 6 in the western U.S. Seismic moments were determined for 272 events which averaged over a wide range of tectonic regions (California, Nevada, Arizona, Utah and Baja California). These were found to be best fit by the curve given by the equation

$$\log M_0 = 1.7\, M_L + 15.1 \qquad 3 < M_L < 6$$

Using the M_S - M_L relationship given by Wyss and Brune (1968), this becomes in terms of $M_S(G)$ (the surface wave magnitude defined by Gutenberg (1945))

$$\log M_0 = M_S(G) + 19.2 \qquad 3 < M_S < 6 .$$

This definition can be compared with the relationship derived directly from Gutenberg's (1945) definition of surface wave magnitude. According to that definition, a magnitude 6 earthquake produces a far-field displacement of $100\mu m$ at distance 22° for surface waves of period 20 seconds. In terms of moment Gutenburg's relationship becomes

$$\log M_0 = M_S(G) + 19.3 .$$

This point thus represents average of the numerous observations on which the surface wave magnitude was based. As pointed out by Richter (1958), the scale was adjusted to agree with the local magnitude values of 6 to 7. Tucker and Brune (1977) did not explicitly give a relationship between surface wave magnitude and seismic moment. However, from the values given in their Tables 1 and 3, the average relationship is

$$\log M_0 = M_S + 19.3 .$$

This relationship, determined using a Gutenburg continental earth model and the Marshall-Basham definition of surface wave magnitude, is in good agreement with the relationship based on the Gutenburg definition of surface wave magnitude. Comparing these various relationships between M_s and M_0 we conclude that the use of the Great Basin velocity (Priestley and Brune, 1978) and attenuation (Patton and Taylor, 1984) model has increased the estimated moment of the

events by 26% over that determined for the Gutenburg continental model.

Equation (3) allows us to rapidly determine the seismic moment M_0 from the surface wave magnitude observation in Table 1. The resulting values of seismic moment (see Table 1) were converted to an equivalent value of Ω_0 by solving equation (1) for Ω_0 and substituting the seismic moment derived from the surface wave observations. This gives values of Ω_0 at frequencies of the surface waves for comparison with the spectra obtained from the body-wave record on the accelerometers.

Error analysis: Errors in Ω_0 (and consequently in M_o) were estimated by calculating an average spectral value and a standard deviation where more than one recording was available for an event. The average values of Ω_o was determined by the formula

$$< \Omega_0 > = antilog \left\{ \frac{1}{NS} \sum_{i=1}^{NS} \log \left[\Omega_{0_i} R_i / 10 \right] \right\}$$

where Ω_{0_i} is the long-period spectral level at the i^{th} station , R_i is the distance to the i^{th} station, and NS is the number of stations recording the event. The standard deviation of the log average value of Ω_o was determined by the formula

$$s.d. (\log < \Omega_o >) = \left\{ \frac{1}{NS-1} \sum_{i=1}^{NS} \left[\log (\Omega_o) - \log < \Omega_o > \right]^2 \right\}^{1/2} .$$

A multiplicative error factor is then determined from

$$E\,\Omega_0 = antilog \left\{ s.d. (\log < \Omega_o >) \right\} .$$

As pointed out by Archuleta *et al.* (1982), when calculating average values of Ω_0 or its derivative M_0, it is necessary to compute the averages using the equations in the above forms to give equal weight to each observation. If a simple arithmetical average value is determined it will be biased toward larger values, since the errors associated with Ω_0 are lognormally distributed.

Observed Spectra: Figures 2 and 3 are displacement spectra for two events of the 24 Mammoth Lakes earthquakes we studied. All spectra are computed from strong-motion accelerograms of the USC-CIT data set. The plotted spectra are the vectorial average of the two orthogonal components, and have been normalized to a hypocentral distance of 10 km. The arrows indicate our picks of the corner frequency and long-period spectral level. The triangle with error bars denotes the average spectral level determined from the surface wave measurements.

Figures 2a-b are two of 14 spectra for an M_L 4.9 event occurring at 1516 UT on May 31, 1980 (hereafter referred to as 5/31/80--1516). The focus of this event is nearly identical to that of the 5/25/80--1633 event. The average value of the long-period spectral level $< \Omega_o >$ measured from the 14 spectra is 1.03×10^{-1} cm-sec, corresponding to $M_o = 1.34 \times 10^{23}$ dyne-cm. Our values include esimates of Ω_o from the data of Archuleta *et al.* (1982) (six observations), plus eight additional spectra from the USC-CIT strong-motion data. Our value of $< \Omega_o >$ does not differ significantly from their. The seismic moment from the surface wave observation is 1.1×10^{23} dyne-cm which is not significantly different from the body-wave value.

Spectra of the largest earthquake we studied, the 5/27/80--1450 M_L 6

shock, are shown in Figure 3a-b. This event is of particular interest because of the controversy concerning its mechanism. Four values of moment have been published for this event. Archuleta *et al.* (1982) determined a moment of 2.33×10^{24} dyne-cm from the spectral analysis of two locally recorded seismograms. Uhrhammer and Ferguson (1980) estimated a moment of 5.0×10^{24} dyne-cm from the spectra of 51.2 seconds of the broad-band displacement record of the vertical component seismogram at Jamestown, California, 140 km west of Mammoth Lakes. Barker and Langston (1983) inverted seven long-period teleseismic P-waveforms and five long-period teleseismic SH-waveforms to obtain the moment tensor for this event. They found a moment of 1.03×10^{25} dyne-cm and 36% CLVD. Given *et al.* (1982) inverted long-period surface wave from this event and used this result to model the long-period body-waves. They found a moment of 1.10×10^{25} dyne-cm. Our values of 7.26×10^{24} and 7.20×10^{24} dyne-cm for the body- and surface-wave observations, respectively, are somewhat higher than the values reported by Archuleta *et al.* (1982) but in reasonable agreement with the other reported values of moment.

Discussion

Figure 4 is a plot comparing the surface wave moments and body-wave moments of the Mammoth Lakes earthquakes from Table 1. The reference line through the points has unit slope and intercept zero. Those points lying above the line have larger body-wave moments compared to the observed surface wave moment, while those below the line have larger surface-wave moments compared to the observed body-wave moment. Vertical error bars denote the spread in the observed body-wave moment while horizontal error bars denote the spread in the observed surface-wave moment. It is clear from this figure that there are no significant differences between the moments determined at 8 to 20 seconds from surface waves, and the moments determined at periods near 1 second from body-waves. Where we have analysed events in common, our results from the surface wave measurements support the moment estimates of Archuleta *et al.* (1982) and thus their findings of nearly constant stress drop ($\Delta\sigma \sim 50$ bars) for events with seismic moments greater than approximately 1×10^{21} dyne-cm. All of the events we have studied are larger than 1×10^{21} dyne-cm and therefore we cannot substantiate the dependence of stress drop on seismic moment which Archuleta *et al.* (1982) observed for smaller events. However, the wider bandwidth of our spectra permit us to address the problem of the source mechanism controversy surrounding the Mammoth Lakes events.

Aki *et al.* (1977) and Chouet (1981) derive theoretical ground motion in the far and near-feld respectively, due to the extension of a fluid-driven tensile crack embedded in a layered half-space. In both studies, the source was a jerky opening of a channel ahead of the crack tip due to excess pressure of the fluid in the crack. Seismic waves are generated by the vibrations of the newly created crack walls due to the rapid application of excess fluid pressure. Both the far-field and near-field studies show a peaked character to the ground motion spectra, in contrast to "tectonic" earthquake spectra which are flat to some corner frequency and then fall off at higher frequencies. Chouet (1981) varied the model parameters to analyze the effects of fluid compressibility, source depth and structure of the medium on the ground motion. He found that the spectral peaks depend on the source geometry, the medium characteristics, the receiver position, the component of ground motion being studied, and critically on the crack stiffness factor C defined as $C = \frac{b\,L}{d\,\mu}$ where b is the bulk modules of the fluid, L is the full length of the crack, d is the crack width, and μ is the rigidity of the solid. The crack vibrates most easily when the crack is empty ($C = 0$) (see

Aki *et al.*, 1977, Figures 6-9). The spectral peak becomes broadened however when the crack stiffness factor is about 5, implying that the bulk modulus of the magma is low enough to contain bubbles (Aki, 1984). Chouet's (1981) model calculations show a pattern similar to the non-double couple mechanism observed for the largest Mammoth Lakes earthquakes (5/25/80--1633, 5/27/80--1450). Utilizing Chouet's (1981) calculations, Aki (1984) has proposed that these events result from the sudden opening of a channel between two pre-existing fluid-filled cracks, due to a higher fluid pressure in one of the cracks. The pressure in the magma drops due to the increased total crack volume and the crack tip closes as a result.

However, as shown in Figure 4, none of the events we have studied show significant differences in level in the frequency band 0.1 to 1.0 Hz and therefore do not show the spectral peaking predicted by the Aki (1984) model for a low viscosity fluid. Most of the strong-motion and digital recording seismographs for the 5/27/80--1450 event were located to the north of this event thus sampling only a portion of the focal sphere, hence it may be argued that we have sampled that part of the radiation pattern where the peaked nature of the spectrum is least prominent. Figure 5 shows the distribution of spectra for the M_L 4.9 5/31/80--1516 aftershock which occurred in almost the same location as the 5/25/80--1633 M_L 6 event which also had a non-double couple mechanism (Given *et al.*, 1982; Julian, 1983). The focal mechanism from local and regional first-motion data for the 5/31/80-1516 event is from Vetter (written communication, 1984) and is very similar to the solution independently determined by Archuleta *et al.* (1982). Figure 5 shows an upper-hemisphere plot with the northwest and southeast being the compression quadrants. This solution is similar to the focal mechanism given by Cramer and Toppozada (1980) and Ryall and Ryall (1980) from local and regional first motion data for the 5/25/80--1633 event. The location of the stations from which the spectra were computed are indicated on the focal sphere. Some of the individual spectra show a suggestion of peaking near 1 Hz, but not of the magnitude predicted by Aki *et al.* (1977) and Chouet (1981). We find nothing in the spectra of the Mammoth Lakes events we have studied which distinguish them from spectra of "tectonic" events observed in numerous previous studies. The flat nature of the spectra does not rule out the opening of a tensile crack as the source of the elastic waves for these earthquakes. It does preclude the opening of a tensile crack with the subsequent injection of a fluid of low viscosity.

Summary

Spectra for 24 Mammoth Lakes earthquakes greater than 1×10^{21} dyne-cm, including the M_L 6 event occurring at 1450 UT on May 27, 1980, have been determined. The short-period portion of the spectra (0.5 - 10.0 Hz) have been determined from spectral analysis of the locally recorded strong-motion and broadband digital data. A relationship has been derived between the Marshall-Basham surface-wave magnitude and seismic moment allowing us to determine the seismic moment directly from time domain amplitude measurements of the surface waves recorded at regional stations. This gives an estimate of the seismic moment independent of that obtained from the S-wave spectra and one based on lower frequencies (0.05 - 0.125 Hz). A comparison of the seismic moments indicate that for any one event, no significant difference in the spectral level exist between the values determined at surface wave frequencies (0.05 to 0.125 Hz) and the S-wave corner frequency (1 to 5 Hz). The events studied, and in particular the 5/27/80--1450 M_L 6 event, do not show peaked spectra predicted from theoretical analysis of the ground motion resulting from a fluid-driven, propagating tensile crack. We have found nothing in the spectra of these events to

distinguish them from "tectonic" earthquakes. The absence of a peaked spectrum does not rule out dike injection as the source of these earthquakes, but it does rule out a particular model of magmatic intrusion, namely that of Chouet (1981) and Aki (1984), for a low viscosity fluid. As Aki (1984) has pointed out, the opening of a channel between two pre-existing fluid filled cracks would largely alleviated this problem by involving the movement of only minor amounts of viscous material, which could be accomplished in an adequately small time.

Acknowledgments

This research was partly suported by the Defense Advanced Research Projects Agency of the Department of Defense and monitored by the Air Force Office of Scientific Research under contract F49620-83-C-0012 (KP), and by the National Science Foundation under grant CEE-8319620 (JB and JA). R.J. Archuleta supplied spectra from the U.S. Geological Survey data, and A.F. Shakal and B.E. Tucker supplied stong-motion records from the California Strong Motion Instrumentation Program. The authors wish to thank D.E. Chavez and A.S. Ryall for a careful review of the manuscript.

References

Abe, K., Seismic displacement and ground motion near a fault: The Saitama earthquake of September 21, 1931, *J. Geophys. Res.*, *79*, 4393-4399, 1974

Aki, K., Evidence for magma intrusion during the Mammoth Lakes earthquakes of May, 1980 and implications of the absence of volcanic (harmonic)tremor, *J. Geophys. Res.*, *89*, 7689-7696, 1984.

Aki, K., M. Fehler, and S. Das, Source mechanism of volcanic tremor: Fluid-driven crack models and their applications to the 1963 Kilauea eruption, *J. Volcanol. Geotherm. Res.*, *2*, 259-287, 1977.

Aruchuleta, R.J., E. Cranswick, C. Mueller, and P. Spudich, Source parameters of the 1980 Mammoth Lakes, California, earthquake sequence, *Geophys. Res.*, *87*, 4595-4607, 1982.

Bailey, R.A., G.B. Dalymple, and M.A. Lanphere, Volcanism, structure and geochronology of Long Valley caldera, Mono County, California, *J. Geophys. Res.*, *81*, 725-744, 1976.

Barker, J.S., and C.A. Langston, A teleseismic body wave analysis of the May 1980 Mammoth Lakes, California, earthquakes, *Bull. Seismol. Soc. Am.*, *73*, 419-434, 1983.

Brune, J.N., Tectonic stress and the spectra of seismic shear waves from earthquakes, *J. Geophys. Res.*, *75*, 4997-5009, 1970.

Brune, J.N., Correction, *J. Geophys. Res.*, *76*, 5002, 1971.

Chouet, B., Ground motion in the near field of a fluid-driven crack and its interpretation in the study of shallow volcanic tremor, *J. Geophys. Res.*, *86*, 5985-6016, 1981.

Cramer, C.H., and T.R. Toppozada, A seismological study of the May 1980 and earlier earthquake activity near Mammoth Lakes, California, *Calif. Div. Mines Geol. Spec. Rep., 150*, 91-130, 1980.

Given, J.W., T.C. Wallace and H. Kanamori, Teleseismic analysis of the 1980 Mammoth Lakes earthquake sequence, *Bull. Seismol. Soc. Am., 72*, 1093-1109, 1982.

Gutenburg, B., Amplitudes of surface waves and the magnitudes of shallow earthquakes, *Bull. Seismol. Soc Am., 35*, 3-12, 1945.

Helmberger, D.V., and S.D. Malone, Modelling local earthquakes as shear dislocations in a layered half space, *J. Geophys. Res., 80*, 4881-4888, 1975.

Hill, D.P., Structure of Long Valley caldera from a seismic refraction experiment, *J. Geophys. Res., 81*, 745-753, 1976.

Julian, B.R., Evidence for dyke intrusion earthquake mechanisms near Long Valley caldera, California, *Nature, 303*, 323-325, 1983.

Knopoff, L., and M. Randall, The compensated linear-vector dipole: A possible mechanism for deep earthquakes, *J. Geophys. Res., 75*, 4957-4963, 1970.

Lide, C.S., and A.S. Ryall, Relationship of aftershocks locations and mechanisms of the May, 1980 Mammoth Lakes earthquakes, *Active Tectonic and Magmatic Processes in Long Valley Caldera, U. S. Geol. Survey Open-File Rept.*, 1984.

Marshall, P.D., and P.W. Basham, Discrimination between earthquakes and underground explosions employing an improved M_s scale, *Geophys. J. R. astr. Soc.,28*,431-458, 1972.

Moslem, K., A. Amini, B. Kontic, J. Anderson, and T. Heaton, Accelerograms from the Mammoth Lakes, California earthquake sequence of May - July, 1980 recorded on a temporary array, Rpt No. CE 83-01, Univ. of Southern California, 1983.

Patton, H.J., and S.R. Taylor, Q Structure of the Basin and Range from Surface waves, *J. Geophys. Res., 89*, 6929-6940, 1984.

Priestley, K.F., and J.N. Brune, Surface waves and the structure of the Great Basin of Nevada and western Utah, *J. Geophys. Res., 83*,2265-2272, 1978.

Richter, C.F., *Elementary seismology* 768pp., Freeman & Co., San Francisco, 1958.

Ryall, A., and F. Ryall, Spatial-temporal variations in the seismicity preceding the May, 1980, Mammoth Lakes, California, earthquakes *Calif. Div. Mines Geol. Spec. Rep., 150*, 27-39, 1980.

Solomon, S., and B. Julian, Seismic constraints on ocean-ridge mantle structure: Anomalous fault plane solutions from first motions, *Geophys. J. R. astron. Soc., 38*, 265-285.

Thatcher, W., and T.C. Hanks, Source parameters of Southern California earthquakes, *J. Geophys. Res.*, *78*, 8547-8576, 1973.

Tucker, B.E., and J.N. Brune, Source mechanism and $m_b - M_s$ analysis of aftershocks of the San Fernando earthquake, *Geophys. J. R. astr. Soc.*, *49*, 371-426, 1977.

Turpin, C.D., Strong-motion instrumentation program results from the May, 1980, Mammoth Lakes, California earthquake sequence, *Calif. Div. Mines Geol. Spec. Rep.*, *150*, 75-90, 1980

Uhrhammer, R.A., and R.W. Ferguson, The 1980 Mammoth Lakes earthquake sequence *Calif. Div. Mines Geol. Spec. Rep.*, *150*, 131-136, 1980.

Vetter, U.R. and A.S. Ryall, Systematic change of focal mechanisms with depth in the western Great Basin, *J. Geophys. Res.*, *88*, 8237-8250, 1983.

Wallace, T., J. Given, and H. Kanamori. A discrepancy between long- and short-period mechanisms of earthquakes near the Long Valley caldera, *Geophys. Res. Lett.*, *9*,1131-1134, 1982.

Wallace, T.C., A re-examination of the moment tensor solutions of the 1980 Mammoth Lakes earthquakes, *Active Tectonic and Magmatic Processes in Long Valley Caldera, US Geol. Survey Open-File Rept.*, 1984.

Wyss, M., and J.N. Brune, Seismic moment, stress, and source dimensions for earthquakes in the California Nevada region, *J. Geophys. Res.*, *73*, 4681-4694, 1968.

Figure Captions

Figure 1. Location maps showing the events studied and the stations from which seismograms were analysed. In the lower right-hand map, the solid circles denote locations of events, triangles denote location of strong-motion accelerographs, and squares denote location of digital seismographs. The upper left-hand map shows the locations of the long-period seismographs used for the surface wave analysis.

Figure 2. Spectra from strong-motion recordings at the sites "McGee Creek Inn" and "Long Valley Fire Station" for the M_L 4.9 event occurring at 1516 UT on May 31,1980. Spectra are the vectorial sum of the two orthogonal components, and have been normalized to 10 km. The long-period spectral level picked from these spectra are denoted by the arrow, and the long-period spectral level determined from the surface-wave observations are denoted by the triangle with error bars.

Figure 3. Spectra from strong-motion recordings at the sites "Cash Baugh Ranch" and "Long Valley Fire Station" for the M_L 6.2 event occurring at 1450 UT on May 27,1980. The notation is the same as for figure 2.

Figure 4. Comparison of the body-wave and surface-wave determined moments for the 24 events studied. The line is for reference and is of unit slope and zero intercept.

Figure 5. Variation of the spectra for the event occurring at 1516 UT on May 31, 1980, as a function of position on the focal sphere. The focal mechanism is from Vetter (written communication, 1984).

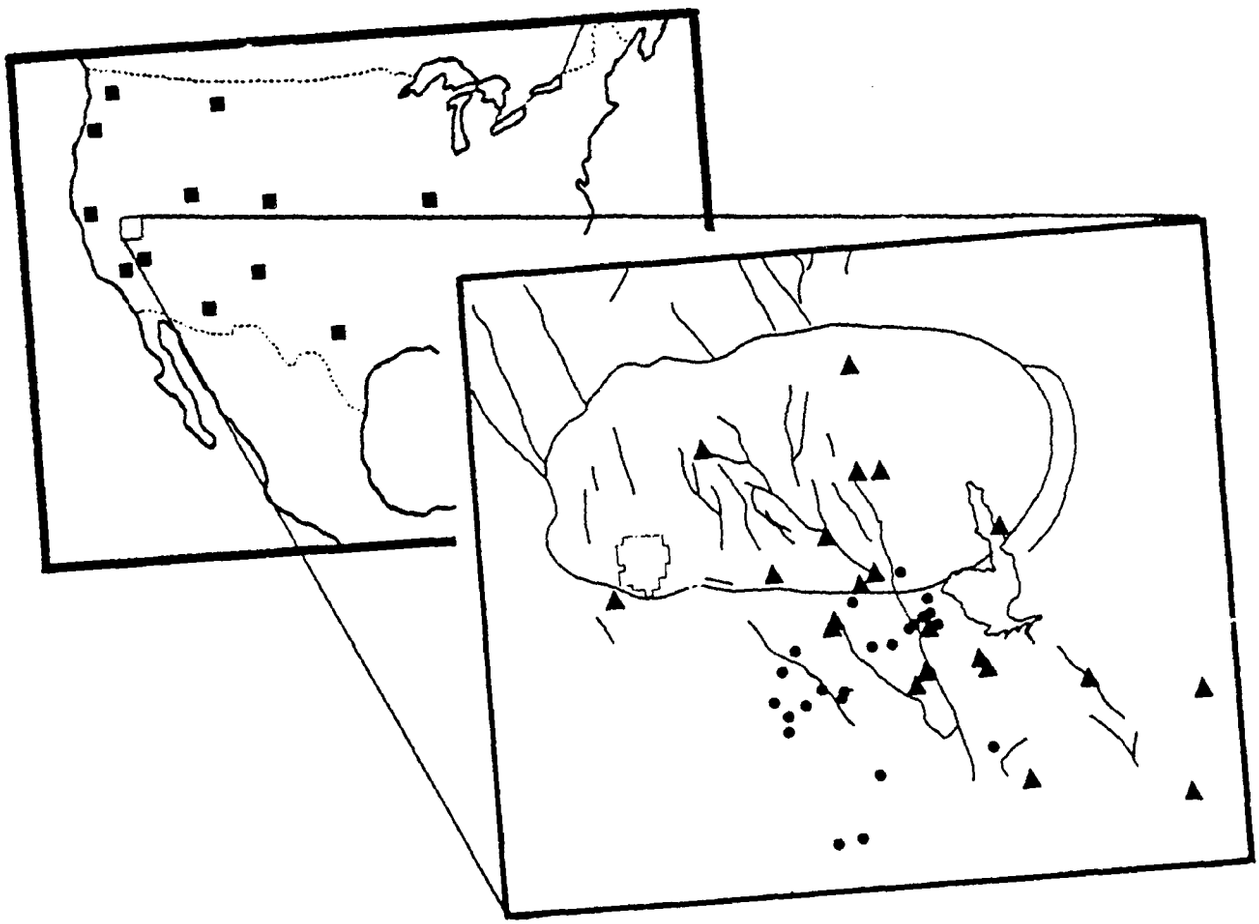

FIGURE 1

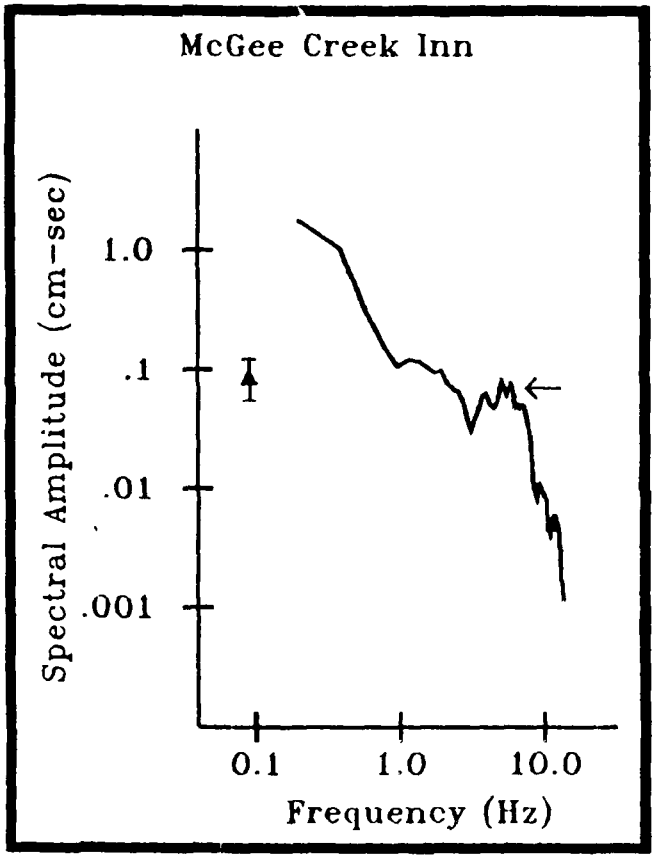
McGee Creek Inn
Spectral Amplitude (cm-sec)
1.0
.1
.01
.001
0.1
1.0
10.0
Frequency (Hz)

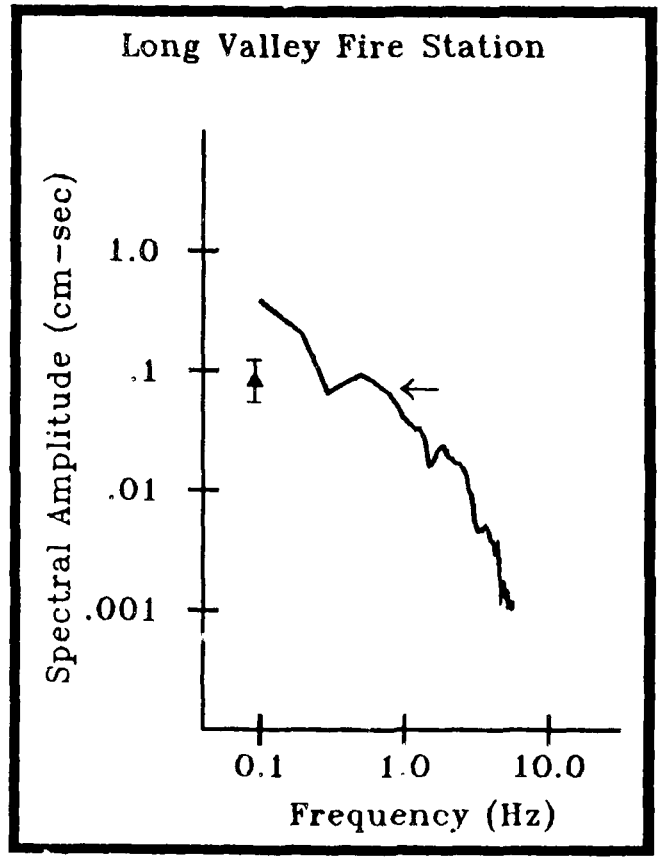
Long Valley Fire Station
Spectral Amplitude (cm-sec)
1.0
.1
.01
.001
0.1
1.0
10.0
Frequency (Hz)

FIGURE 2

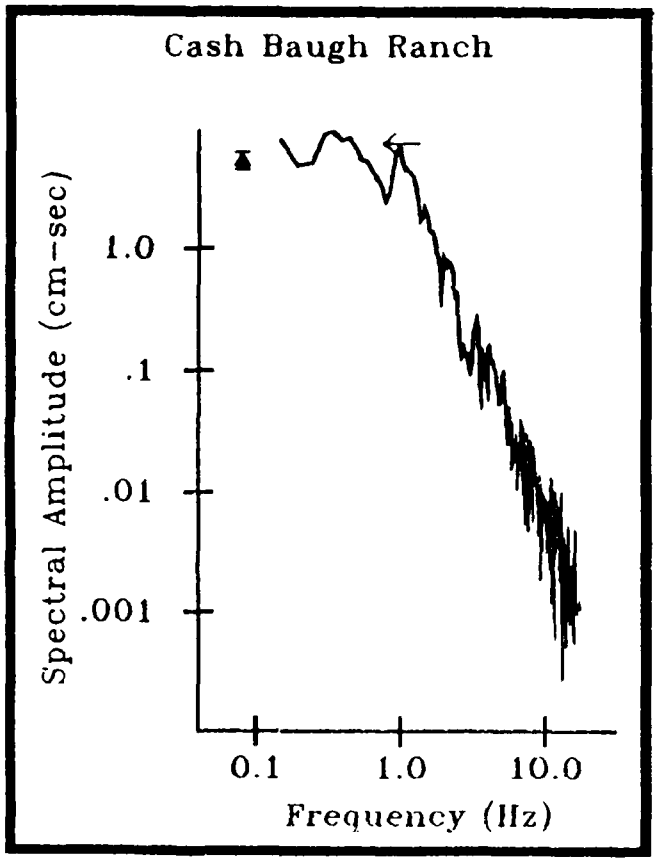
Cash Baugh Ranch
Spectral Amplitude (cm-sec)
1.0
.1
.01
.001
0.1
1.0
10.0
Frequency (Hz)

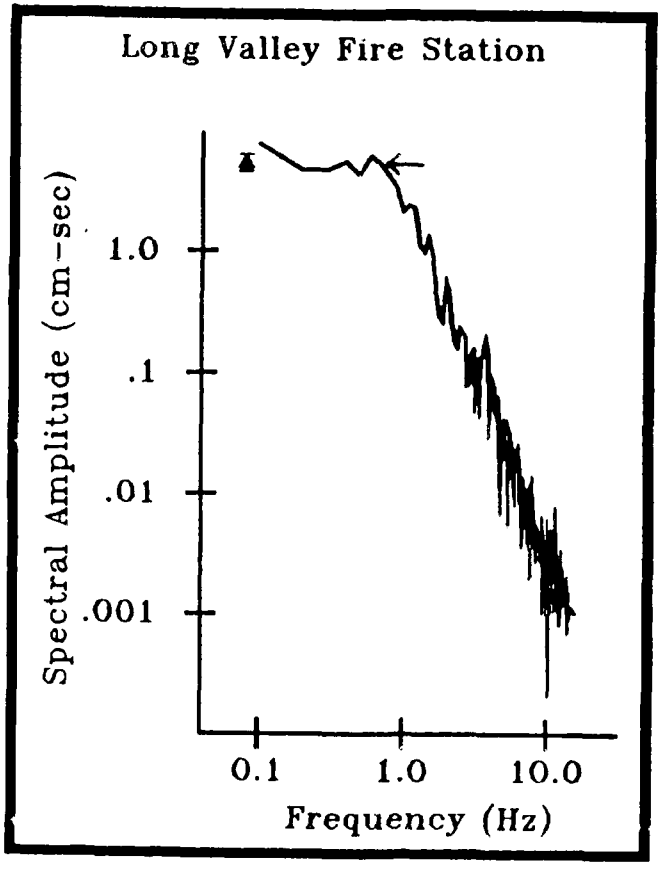
Long Valley Fire Station
Spectral Amplitude (cm-sec)
1.0
.1
.01
.001
0.1
1.0
10.0
Frequency (Hz)

FIGURE 3

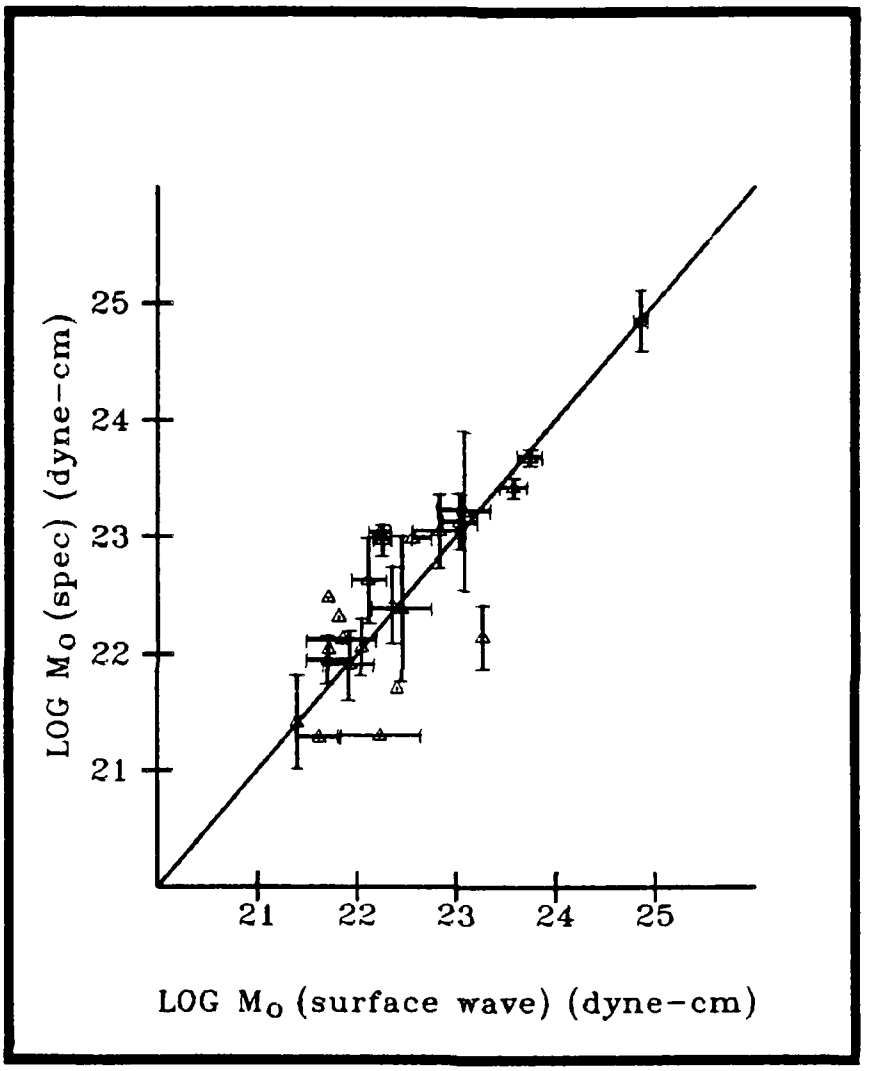
LOG Mo (spec) (dyne-cm)
25
24
23
22
21
21
22
23
24
25
LOG Mo (surface wave) (dyne-cm)

FIGURE 4

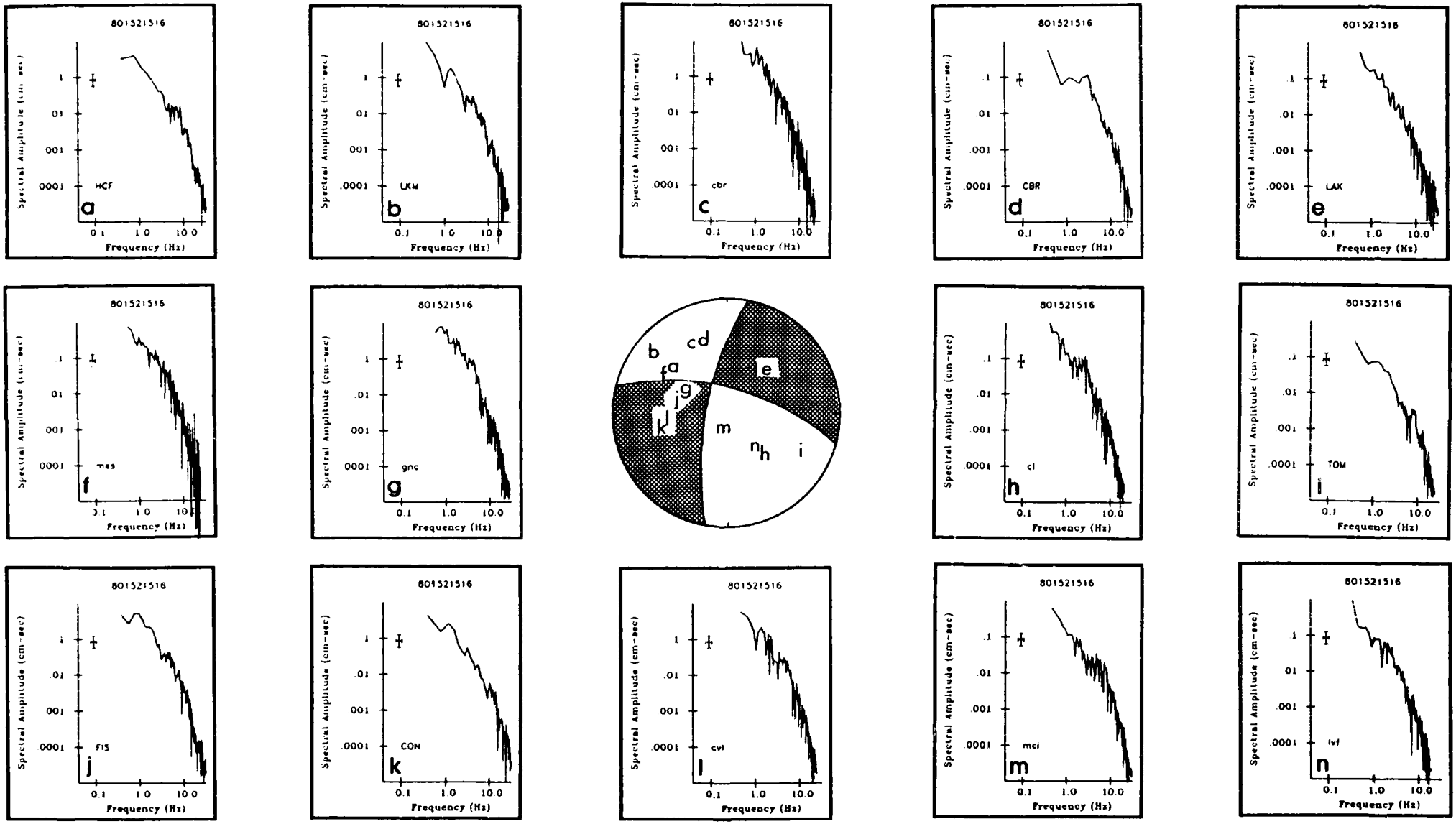
801521516
Spectral Amplitude (cm-sec)
Frequency (Hz)
HCF
a
801521516
LKM
b
801521516
cbr
c
801521516
CBR
d
801521516
LAK
e
801521516
mas
f
801521516
gnc
g
b
cd
fa
e
g
j
k
l
m
nh
i
801521516
cl
h
801521516
TOM
i
801521516
FIS
j
801521516
CON
k
801521516
cvl
l
801521516
mcl
m
801521516
lvf
n

FIGURE 5

A COMPARISON OF THE SHORT AND LONG PERIOD SPECTRAL SOURCE PROPERITIES OF THE 1980 MAMMOTH LAKES EARTHQUAKE SEQUENCE

Keith F. Priestley

Seismological Laboratory, University of Nevada, Reno, NV 89557

James N. Brune

Institute of Geophysics and Planetary Physics
Scripps Institution of Oceanography
University of California, San Diego
La Jolla, California 92093

Introduction

Earthquakes with similar short-period amplitudes, as evidenced by similar local magnitude M_L, can show large differences in long-period amplitudes. These differences can arise due to variations in the properties of the path, the source depth, and source parameters. Understanding the differences in the relative excitation of high frequency (0.5-10.0 Hz) and low frequency (0.05-0.125 Hz) seismic waves, and the propagation of this energy at regional distance, is important for understanding source mechanisms, and more specifically for evaluating the possibilities of discriminating small explosions from earthquakes at regional distance. The $m_b - M_s$ discriminant, which compares the relative excitation of body versus surface waves, is presently one of the primary techniques for distinguishing explosions from earthquakes. The theoretical basis for the discriminant is still not well understood, it is thought to arise from differences in one or several of the following source parameters: (1) source dimension, (2) source rupture duration, (3) time function of the displacement at various points on the fault for an earthquake or at the elastic radius for an explosion, and (4) source symmetry.

Regional variations in the relative excitation of high and low frequency seismic waves generated by earthquakes in western North America have been noted in a number of studies. Brune, Espinosa and Oliver (1963) found a wide range in the surface wave excitation, for a given ML, for earthquakes in the California-Nevada region. Wyss and Brune (1968) found that earthquakes in Nevada often generated smaller amplitude surface waves for a given M_L, than do earthquakes along the San Andreas fault or along the northern California coast. In a later study, Wyss and Brune (1971) noted large differences in the ratio of Gutenburg energy E_G determined from M_L, with seismic moment M_0 determined from surface waves, for earthquakes in the California region. In particular, they found high values of apparent stress ($\mu E_G / M_0$) for earthquakes in the region north of Bishop, California. At that time it was not possible to assess the effects of variations in source depth and source mechanism.

This study is concerned with the relative excitation of seismic energy in the band 0.05-10.0 Hz from earthquakes in the 1980 Mammoth Lakes, California, sequence. These earthquakes have been studied more thoroughly than perhaps

any other earthquake sequence in the western United States. A large number of broad-band digital and strong-motion recordings have been collected in the epicentral region, and a dense network of high-gain seismographs provide data for accurate hypocentral coordinates and first motions for most events. The epicentral region is surrounded by a network of long-period seismographs, and is at a distance of 20°–30° from the high gain stations of the Canadian Network. Finally, in the context of seismic discrimination, the events are in a similar tectonic environment to the Nevada Test Site, approximately 150 km to the southeast. Thus the effects of structure on seismic wave propagation, especially to the east, should be similar for both earthquakes at Mammoth Lakes and explosions at the Nevada Test Site.

Data

This study is based on seismograms of the Mammoth Lakes earthquakes shown in Figure 1. These events comprise only a small fraction of the total number of events which have occurred in the Mammoth Lakes area since the earthquake sequence began in October, 1978. Those selected for study consist ones for which both strong-motion or digital local recordings and long-period regional recordings exist. All events have been located using arrival times from the local stations shown in Figure 1, with additional readings from local stations operated by the University of Nevada and the California Institute of Technology. We have obtained first-motion focal mechanisms for a number of the events from Vetter (personal communications, 1984).

Seismograms used in this study are from the seismograph stations shown in Figure 1. The SMA-1 strong-motion accelerographs were installed by the California Division of Mines and Geology (Turpin, 1980), or by the University of Southern California (Moslem *et al.*, 1983). Digital stations described by Archuleta *et al.* (1982), consist of either force-balance accelerometers or velocity transducers and Sprengnether DR-100 recorders. These stations are denoted by triangles in Figure 1. For events along the southern boundary of the caldera, the SMA-1 and digital seismographs cover a larger fraction of the focal sphere than many previous studies of a similar nature. The radiation pattern of events south of the caldera is not as well sampled, however.

Figure 1 also shows the locations of the regional long-period stations (denoted by squares) from which seismograms were used to determine surface wave magnitudes. These stations completely surround the Mammoth Lakes region and are all WWSSN stations with the exception of the California Institute of Technology station at Pasadena (PAS). Readings from the Canadian network stations (denoted by stars) were used to determine body wave magnitude.

Magnitude Analysis

Local magnitude (M_L) for the main shocks and larger aftershocks are reported from Wood-Anerson amplitude measurements at the University of California-Berkeley and the California Institute of Technology. M_L for the smaller events are taken from Chavez and Priestley (1985).

The *Earthquake Data Reports* of the U.S. Geological Survey report peak-to-peak amplitude, period, and individual station body-wave magnitude (m_b). From this listing we have tabulated the body-wave magnitude reported by Canadian Network stations at distances greater than 20° from Mammoth Lakes, and from these values we have determined an average m_b value for the 37 Mammoth Lakes earthquakes studied.

We have determined the surface wave magnitude using the definition of Marshall and Basham (1972). This value of M_s is defined by the equation

$$M_s = \log A + B(\Delta) + P(T) \quad (1)$$

where A is one-half the peak-to-peak ground amplitude of the maximum Rayleigh wave with a period T at a distance Δ. $B(\Delta)$ is a correction for the average effects of attenuation, scattering, geometrical spreading and refraction; P(T) is a correction factor for dispersion which allows measuring the surface wave amplitude over a range of periods. Marshall and Basham (1972) have tabulated P(T) for continental North America for periods ranging from 10 to 40 seconds. In some cases the maximum surface wave amplitude observed for the Mammoth Lakes earthquakes was in the range 8 to 10 seconds, however since P(T) is a smoothly varying function, we have extrapolated P(T) to 8 seconds period. Marshall and Basham have also provided for correcting M_s for source depth by comparing M_s determined for an event at different periods. However, most of the surface wave observations made here consist of a single Airy phase, and thus such a comparison could not be made.

Long-period seismograms from all western United States WWSSN stations and the long-period station at Pasadena were examined. Equ (1) was used to determine the M_s from eqn (1) for each station. From these values, we determined an average M_s for each event.

Figure 2 compares the $m_b - M_s$ to the North American earthquake and explosion data of Marshall and Basham (1972). Magnitudes in the latter study were determined from seismograms recorded on Canadian Network stations. In this study Canadian Network data were used to determine m_b, while data from long-period stations in the western U.S. were used to determine M_s. This could lead to a systematic difference between the M_s determined by Marshall and Basham, and the M_s determined for the Mammoth Lakes earthquakes. This does not seem to be a strong effect, since the paths overlap to a large extent, and the data sets in Figure 2 overlap as well. Neither the Marshall-Basham data nor the Mammoth Lakes earthquakes data have been corrected for depth variations. All Mammoth Lakes events fall within the earthquake population and discriminate from explosions, although some events are well-offset from the earthquake mean towards the explosion population.

Body-wave estimates of source parameters

The seismograms analyzed display varying degrees of complexity, ranging from simple pulses to wave trains several seconds long. This variation is possibly a consequence of the position of the station on the focal sphere. For instance, seismograms showing large, simple S-waves often have relatively small P-wave amplitudes. In this case, if the S-wave amplitude is large, it will exceed the scattered energy and the resulting seismogram will have a simpler character. In some cases, it is apparent from the long period oscillations following the S-wave, that earth structure contributes to the complexity of the seismograms. Displacement amplitude specta were computed for these locally recorded body-wave data. The SMA-1 analog seismograms were digitized at a sample interval of 0.025 sec; the digital recordings supplied from the U.S. Geological Survey were digitized at an interval of 0.05 sec. Displacement amplitude spectra were computed by Fourier transforming the S-wave arrival, correcting for instrument response, and dividing the acceleration spectra by ω^{-2} and the velocity spectra by ω^{-1} to give displacement spectra. Time windows were chosen to be long enough to include the entire S-wave arrival, but short enough to minimize the inclusion of surface wave energy. The spectra have been normalized to a

distance of 10 km. Rather than rotate the data into radial and transverse components, we took the vector sum of the two horizontal component spectra.

The spectra were interpreted in terms of a flat, low-frequency asymptote, Ω_0, a high frequency falloff with a slope in the range ω^{-1} to ω^{-3}, and the corner frequency f_c at which the two trends intersect. In almost all cases, there is a second corner in the data at frequencies between 10 and 16 Hz. Below this frequency the spectra drop off as ω^{-4} to ω^{-5}. This frequency may represent the f_{max} of Hanks (1982). The asymptotes were fit by eye using an interactive computer routine. This method of fitting is subjective and a more rigorous technique could be adopted such as fitting the asymptotes by a least-squares type procedure. However, the simple technique used here is felt to be adequate because its errors were smaller than other known errors involved in estimating Ω_0 and f_c. Figure 3 is an example of this estimation of the fits for one seismogram.

The far-field spectral parameters were then related to the source parameter seismic moment M_0 using the relationship given by Brune (1970, 1971)

$$M_0 = \frac{4\pi\rho\beta^3\Omega_0 r}{kR_{\vartheta\varphi}} \tag{2}$$

where ρ is the density ($\rho = 2.8\ g\ cm^{-3}$), β is the shear-wave velocity ($\beta = 3.5\ km\ s^{-1}$), r is the hypocentral distance, $R_{\vartheta\varphi}$ is the RMS average of the radiation pattern (taken here as 0.6), and k is a correction factor for the amplification of SH waves at the free surface (taken as 2). The correction of the amplitude of the S-wave on being reflected at the free surface assumes that the waves are horizontally polarized (SH), however since we have not rotated the data into transverse and radial components, the data are in general some mixture of SH and SV motion. Abe (1974) discusses experimental studies of amplification on reflection and concludes that using $k = 2$ applies approximately to SH-wave signals containing some SV motion. Helmberger and Malone (1975) discuss problems due to multiple arrivals caused by reflections in deducing source parameters from S-waves recorded at epicentral distances much greater than the source depth. The station-source configuration shown in Figure 1 indicates that this should not be a problem in this study.

A source of error inherent in the estimate of Ω_0, and consequently in the estimates of M_o, comes from the assumption of a single, average correction for radiation pattern. If sufficient instruments were available, or if the source parameters including direction and velocity of rupture were known, this error could be reduced. A value of 0.6 was used for $R_{\vartheta\varphi}$ (Thatcher and Hanks, 1973). At some azimuths, the amplitude could be 1.67 times larger than the amplitude determined assuming this correction, while near a node in the radiation pattern the amplitude could be quite small. Furthermore, if the source dimension is comparable to the wavelength involved, source propagation might distort the radiation pattern by focusing or defocusing energy, thereby changing the apparent corner frequency for different directions and possibly reducing the calculated moment.

No Q correction was made in determining the spectra. Archuleta *et al.* (1982) found that whole-path Q had a small effect on the measurement of Ω_0 for Mammoth Lakes events.

Errors in Ω_0 (and consequently in M_o) were estimated by calculating an average spectral value and a standard deviation where more than one recording was available for an event. The average values of Ω_o were determined by the formula

$$< \Omega_0 > = antilog \left\{ \frac{1}{NS} \sum_{i=1}^{NS} \log \left[\Omega_{0_i} R_i / 10 \right] \right\} \quad (3)$$

where Ω_{0_i} is the long-period spectral level at the i^{th} station , R_i is the distance to the i^{th} station, and NS is the number of stations recording the event. The standard deviation of the log average value of Ω_0 was determined by the formula

$$s.d. (\log < \Omega_0 >) = \left\{ \frac{1}{NS-1} \sum_{i=1}^{NS} \left[\log (\Omega_0) - \log < \Omega_0 > \right]^2 \right\}^{1/2} . \quad (4)$$

A multiplicative error factor is then determined from

$$E \Omega_0 = antilog \left\{ s.d. (\log < \Omega_0 >) \right\} . \quad (5)$$

As pointed out by Archuleta *et al.* (1982), when calculating average values of Ω_0 (or M_0), it is necessary to compute the averages using the equations in the above forms to give equal weight to each observation. If a simple arithmetical average value is determined it will be biased toward larger values, since the errors associated with Ω_0 are lognormally distributed.

Determination of Surface Wave Moment

Tucker and Brune (1977) used surface wave spectra of the San Fernando aftershocks to obtain estimates of seismic moments which were independent of those indicated by the S-wave spectra, and which sampled a lower frequency portion of the spectrum. For a number of large eventsmoments determined at the surface wave periods indicated that the low-frequency part of the spectrum is roughly proportional to ω^{-1}. Reexamination of the near-source spectra for these events were in fact, found to be rising towards lower frequency in contrast to the spectra for almost all other events. They made a careful estimate of the errors involved in estimating the seismic moment from the surface wave spectra. The errors included procedural errors, path structure and attenuation, lateral refraction (multipathing), source finiteness, and uncertainties in fault parameters (depth, dip, strike, and slip vector) in correcting for the radiation pattern. They concluded that these effects could lead to a maximum error in the final result of no more than a factor of 4.

In this study we also determined the seismic moment from surface waves for comparison with seismic moments determined from the S-wave spectra, however we used a different procedure which allowed us to determine the seismic moment from a large number of events without the time-consuming digitization of the surface wave seismograms. Surface wave synthetics were generated by a computer routine (written by Guy Masters) for an earthquake with $M_0 = 10^{21}$ dyne-cm at a number of regional seismographs from which data were used to determine the surface-wave magnitudes. From the synthetic surface wave seismograms, we determined the surface wave magnitude in the same manner as discussed above for the Mammoth Lakes earthquakes, and thus determined a linear relationship between the surface wave magnitude and the logarithum of the seismic moment.

Factors affecting the calculation of the synthetic surface wave seismograms are the earth velocity and attenuation structure and the fault parameters of the individual earthquakes. Since the events are located at the western edge of the Great Basin, while most of the seismograph stations are located in western North

America, we have used the velocity structure determined for the Great Basin from surface wave dispersion measurements (Priestley and Brune, 1978). The attenuation structure for the Great Basin by Patton and Taylor (1984) was used, with a slight lowering of Q_β from that of Patton and Taylor in the surficial layer. Since we do not have fault-plane solutions nor do we know the focal depth for the majority of events we have studied, we determined an average relationship for the Mammoth Lakes area in the following manner. Vetter and Ryall (1983) have determined fault plane solutions for a large number of events in the Mammoth Lakes area, and found that the mechanisms can generally be divided into two groups. The first group consists of earthquakes with strike-slip mechanisms (average plane of strike N14°E, dip 80°ESE, slip N16°E or strike N73°W, dip 80°SSW, slip N76°E) which are most commonly at depths less than 9 km. The second group consists of earthquakes with oblique or normal mechanisms (average planes of strike N03°E, dip 64°E, slip N40°E or strike N50°W, dip 38°SW, and slip N86°W) usually at depths greater than 9 km. Synthetic surface wave seismograms were calculated for both mechanisms for 2, 5, 8, 11 and 14 km depth. Surface-wave magnitudes were determined from the 10 records at each station and an average conversion factor determined for both focal mechanisms and all focal depths. The resulting relationship between surface wave magnitude M_S and seismic moment M_0 for the Mammoth Lakes area is given by the equation

$$\log M_0 = M_S + 19.40(\pm 0.06) . \tag{5}$$

To verify the validity of our moment-surface wave magnitude relationship, we can compare equation (5) with other similar relations established for the western United States. Wyss and Brune (1968) originally established a moment-local magnitude relationship for events less than magnitude 6 in the western U.S. Seismic moments were determined for 272 events which averaged over a wide range of tectonic regions (California, Nevada, Arizona, Utah and Baja California). These were found to be best fit by the curve given by the equation

$$\log M_0 = 1.7\, M_L + 15.1 \qquad 3 < M_L < 6 \tag{7}$$

Using the M_S - M_L relationship given by Wyss and Brune (1968), this becomes in terms of $M_S(C)$ (the surface wave magnitude defined by Gutenberg (1945))

$$\log M_0 = M_S(C) + 19.2 \qquad 3 < M_S < 6 . \tag{8}$$

This definition can be compared with the relationship derived directly from Gutenberg's (1945) definition of surface wave magnitude. According to that definition, a magnitude 6 earthquake produces a far-field displacement of $100\mu m$ at distance 22° for surface waves of period 20 seconds. In terms of moment Gutenburg's relationship becomes

$$\log M_0 = M_S(C) + 19.3 . \tag{9}$$

This point thus represents average of the numerous observations on which the surface wave magnitude was based. As pointed out by Richter (1958), the scale was adjusted to agree with the local magnitude values of 6 to 7. Tucker and Brune (1977) did not explicitly give a relationship between surface wave magnitude and seismic moment, however from the values given in their Tables 1 and 3, the average relationship is

$$\log M_0 = M_S + 19.3 . \tag{10}$$

This relationship, determined using a Gutenburg continental earth model and the Marshall-Basham definition of surface wave magnitude, is identical to the relationship based on the Gutenburg definition of surface wave magnitude. Comparing these various relationships between M_s and M_o we conclude that the use of the Great Basin velocity (Priestley and Brune, 1978) and attenuation (Patton and Taylor, 1984) model has increased the estimated moment of the events by 26% over that determined for the Gutenburg continental model.

Equation (6) allows us to rapidly determine the seismic moment M_0 from the surface wave magnitude observation. The resulting values of seismic moment were converted to an equivalent value of Ω_0 by solving equation (2) for Ω_0 and substituting the seismic moment derived from the surface wave observations. This gives values of Ω_0 at frequencies of the surface waves for comparison with the spectra obtained from the body-wave record on the accelerometers. The values of seismic moment are compared in Tapbe 4.

Comparison of short-period and long-period estimates of seismic moment

Figure 4 is a plot of the seismic moment determined from the spectral analysis of the strong-motion and digital data recorded at near distances (Δ < 20 km), and the seismic moment determined from the surface waves recorded at larger distances (Δ > 375 km). The line is of unit slope and zero intercept, and is for reference. As shown in this Figure, most of the events we have studied show no significant differences in the long-period spectral level as measured near frequencies near 1 Hz and as measured near frequencies of 10 Hz. 1.0 Hz. In comparing short period versus long period excitation of events in the California region, Wyss and Brune (1971) found that events occurring to the north of Bishop, California indicated higher apparent stress than events along the San Andreas fault. In a number of recent studies in southern California (Tucker and Brune, 1977; Hartzell and Brune, 1977, 1979), discrepancies have been note between the between long and short period determinations of seismic moments. Such discrepancies may arise due to partial stress drop (Brune, 1970) or to afterslip on the fault (Hartzell and Brune, 1979). In the latter case, the body wave moment, and presumably m_b and M_L, are the result of the breaking of an asperity, while the overall moment, and presumably M_s, is the result of the overall faulting process. We have found such events to be uncommon in the Mammoth Lakes sequence, as is shown in Figure 4. This may arise due to a higher overall state of stress in the crust in the vicinity of Mammoth Lakes.

Comparison of magnitude estimates with source spectra

Six events were chosen for special study. These are events which cover the range of depths and focal mechanisms observed at Mammoth Lakes, and for which we have local data for determination of the spectra, plus determinations of M_L, m_b, and M_s.

In order to compare the similarities and differences in the magnitude estimates for these events, it is important to consider the frequency associated with each measurement. The magnitude values were related to the spectra in the following way. The 801481901 event was chosen as a reference since: (1) both the spectrum and magnitude estimates were well-determined, (2) this was one of the smaller events and thus any effects of fault finiteness are minimized; (3) the event is shallow; and (4) the frequencies at which M_L, m_b, and M_s were determined at are all lower than the corner frequency, i.e., all measurements were from the flat portion of the spectrum. The average spectrum for this event is

shown in Figure 5a. The error bars at the corner of the spectrum denote the range in Ω_o and f_c, and the high frequency slope is the average of all measurements. Additive constants for each of the magnitudes were found such that the magnitude values fall on the spectrum corresponding to their appropriate frequency. The frequency for m_b and M_s is the mean frequency of the magnitude measurements and error bars denote the spread in those measurements. M_L was assumed to be measured at a period of 0.8±0.2 sec., the free period of a Wood-Anderson seismometer

The magnitude measurements were made at similar frequencies for all six earthquakes. The most significant deviation is for m_b where the period for the shallower events is 0.8±0.1 sec and the period for the deepest event, 801471224, is 1.3±0.1 sec. Because all paths to the regional and teleseismic stations were essentially identical, and because of the similarity in the frequency of each of the magnitude measurements, we felt justified in applying the additive constants determined for the 801481901 event to the other five events.

The 801490516 event is similar in magnitude and depth to the reference event. Both events have a similar corner frequency and it is not surprising that M_L and m_b fall below the corner frequency and on the flat portion of the spectrum. The M_s value falls above the long-period level, but this is not significant considering the error bars on M_S and Ω_o.

The event 801471857 is almost one magnitude unit larger than the reference event 801481901, but is of similar depth. The M_s value for this event falls close to the long-period level while both m_b and M_L were measured at frequencies within the error bars f_c. When these values are normalized to the reference event, both fall below the long period level and near the high frequency slope.

Comparison of these three events, 801481901 and 801490516 which are of similar magnitude and depth, and 801471857 which is of similar depth but approximately one magnitude unit larger justifies our rationale of relating the magnitude measurements to the spectrum.

The event occurring at 801462035 has the largest surface wave magnitude of the six event discussed in this section. It is approximately 8 km deep, near the transition zone in focal mechanisms found by Vetter (1984). We have only one strong-motion record for determining the source spectrum, hence there are no error bars on the corner frequency or long-period level. m_b is determined at a frequency lower than the corner frequency, and falls approximately a factor of two below the Ω_o level. M_L is above the corner frequency and not far removed from the high frequency asympote. The M_s value, however, is a factor of 10 greater than the long-period asymptote. This event is approximately 6 km deeper than those discussed above which would somewhat decrease the short period Rayleigh wave excitation. The mean period of the Rayleigh wave Airy phase is slightly longer for this event (12.0±2.5sec) compared to the shallower events (10.0±2.0sec). Such discrepancies between long and short period moments have been observed in a number of similar studies in southern California (Tucker and Brune, 1977; Hartzell and Brune, 1977, 1979). Such a discrepancy may arise due to partial stress drop (Brune, 1970) or to afterslip on the fault (Hartzell and Brune, 1979). In the latter case, the body wave moment, and presumably m_b and M_L, are the result of the breaking of an asperity, while the overall moment, and presumably M_s, is the result of the overall faulting process. We have found such events to be uncommon in the Mammoth Lakes sequence, as is shown in Figure 4.

The event 801471224 occurring at 12.5 km, is the deepest event studied, as well as one of the deepest events of the Mammoth Lakes sequence. For this

event, M_L falls on the high frequency asymptote above the corner frequency, while m_b is at a frequency below the corner and approximately a factor of five beneath the long period level. The M_s error bars intersect the long period level although the average value is slightly below, possibly due to the increased source depth.

The final event examined is that occurring at 801520058. This is the smallest event of the six studied and one of those in Figure 2 which is offset from the earthquake population towards the explosion population. The depth of this event is similar to that of the reference event, so the low value of M_s cannot be attributed to source depth. Both m_b and M_L fall within the corner frequency error bars. Two features of the spectrum of this event distinguish it from the other five events examined. First, the high-frequency slope is nearer to ω^{-1} compared to a high frequency slope of approximately ω^{-2} for the other events. Second, in all of the individual spectra for 801520058, there is a sharp break in slope at about 10 Hz. The other earthquakes also show a second break in slope between 10 and 15 Hz which may represent the same feature. This may be more pronounced for the 801520058 event due to the shallower slope between 1 and 10 Hz. Other than these features, there is nothing to distinguish this event from those which plot along the earthquake trend in Figure 2. All of the six events with the exception of 801520058 have stress drops of the order 100 bars. 801520058 has a stress drop of 15 bars.

The moment and corner frequencies for the 801471857, 801481901 and 801490516 events are all in approximate agreement with the ω^{-2} model for the spectra of earthquakes (Aki, 1967; Brune 1970, 1971). The corner frequency of the 801471857 earthquake is about a factor of 2 lower than 801481901 and 801490516, whereas the corresponding long-period amplitudes of 801471857 are approximately 10 times higher. Thus the corner frequencies and moment of the 801471857, 801181901, and 801490516 are in agreement with the ω^{-2} model for events of approximately the same stress drop, but with source dimensions different by a factor of 2 (Hanks, 1979).

Conclusions

In comparing short period versus long period excitation of events in the California region, Wyss and Brune (1971) found that events occurring to the north of Bishop, California indicated higher apparent stress than events along the San Andreas fault. In this study we have looked in detail at the relative excitation of short and long period energy in this region from aftershocks of the Mammoth Lakes sequence.

We have compared the body wave magnitude, m_b, and surface wave magnitude, M_s, and find that Mammoth Lakes events with few exceptions discriminate from nuclear explosions occurring at the Nevada Test Site approximately 150 km to the southeast.

We have used local strong-motion and broad-band digital recordings to compute the source spectra of 37 earthquakes. For events in common with Archuleta *et al* (1982) our moments are in agreement. We have developed a moment-surface wave magnitude relationship which allows us to rapidly determine the seismic moment at surface wave periods from time domain amplitude measurements on the long-period seismogram. These determinations of moment in almost all cases agree closely with the moments determined from the spectra. Similar studies in southern California show long-period moments exceeding short-period moments by a factor of 4 to 10.

Hartzell, S., and J. Brune, Source parameters for the January 1975 Brawley-Imperial Valley earthquake swarm, *Pageoph, 11*, 333-355.

Helmberger, D.V., and S.D. Malone, Modelling local earthquakes as shear dislocations in a layered half space, *J. Geophys. Res., 80*, 4881-4888, 1975.

Marshall, P.D., and P.W. Basham, Discrimination between earthquakes and underground explosions employing an improved M_s scale, *Geophys. J. R. astr. Soc., 28*,431-458, 1972.

Moslem, K., A. Amini, B. Kontic, J. Anderson, and T. Heaton, Accelerograms from the Mammoth Lakes, California earthquake sequence of May - July, 1980 recorded on a temporary array, Rpt No. CE 83-01, Univ. of Southern California, 1983.

Patton, H.J , and S.R. Taylor, Q Structure of the Basin and Range from Surface waves, *J. Geophys. Res., 89*, 6929-6940, 1984.

Priestley, K.F., and J.N. Brune, Surface waves and the structure of the Great Basin of Nevada and western Utah, *J. Geophys. Res., 83*,2265-2272, 1978.

Richter, C.F., *Elementary seismology* 768pp., Freeman & Co., San Francisco, 1958.

Thatcher, W., and T.C. Hanks, Source parameters of Southern California earthquakes, *J. Geophys. Res., 78*, 8547-8576, 1973.

Tucker, B.E., and J.N. Brune, Source mechanism and $m_b - M_s$ analysis of aftershocks of the San Fernando earthquake, *Geophys. J. R astr. Soc., 49*, 371-426, 1977.

Turpin, C.D., Strong-motion instrumentation program results from the May, 1980, Mammoth Lakes, California earthquake sequence, *Calif. Div. Mines Geol Spec. Rep., 150*, 75-90, 1980

Vetter, U.R. and A.S. Ryall, Systematic change of focal mechanisms with depth in the western Great Basin, *J. Geophys. Res., 88*, 8237-8250, 1983.

Wyss, M., and J.N. Brune, Seismic moment, stress, and source dimensions for earthquakes in the California - Nevada region, *J. Geophys. Res., 73*, 4681-4694, 1968

Wyss, M., and J. Brune, Regional variations of source properties in Southern California estimated from the ratio of short- to long-period amplitudes, *Bull. Seismo. Soc. Am., 61*, 1153-1167.

Figure Captions

Figure 1. Location maps showing the events studied and the stations from which seismograms were analysed. In the lower right-hand map, the solid circles denote locations of events, triangles denote location of strong-motion

accelerographs, and digital seismographs. The upper left-hand map shows the locations of the long-period seismographs used for the surface wave analysis (squares), and Canadian network short-period stations used to determine body-wave magnitude.

Figure 2. Comparison of the body-wave magnitudes surface-wave magnitude. The solid dot (earthquakes) and pluses (explosions) are taken from Marshall and Basham (1972); the solid squares are the Mammoth Lakes events from this study. All body-wave magnitudes are from measurements from Canadian network seismographs. Surface wave magnitudes taken from Marshall and Basham are from Canadian network long-period seismographs, surface wave magnitudes for the Mammoth Lakes earthquakes are from long-period WWSSN stations in the western United States.

Figure 3. Representative analysis of short-period digital seismogram. The bracket over the seismogram indicates the S-wave window; the heavy solid lines indicate the long-period and high-frequency asymptotes fit to the spectrum.

Figure 4. Comparison of the body-wave and surface-wave determined moments for the events studied. The line is for reference and is of unit slope and zero intercept.

Figure 5. Comparison of the source spectra and the determined values of the local magnitude, body-wave magnitude, and the surface wave magnitude at threir appropriate frequencies. The error bars assigned to each spectral value represent the estimated standard error of the measurement.

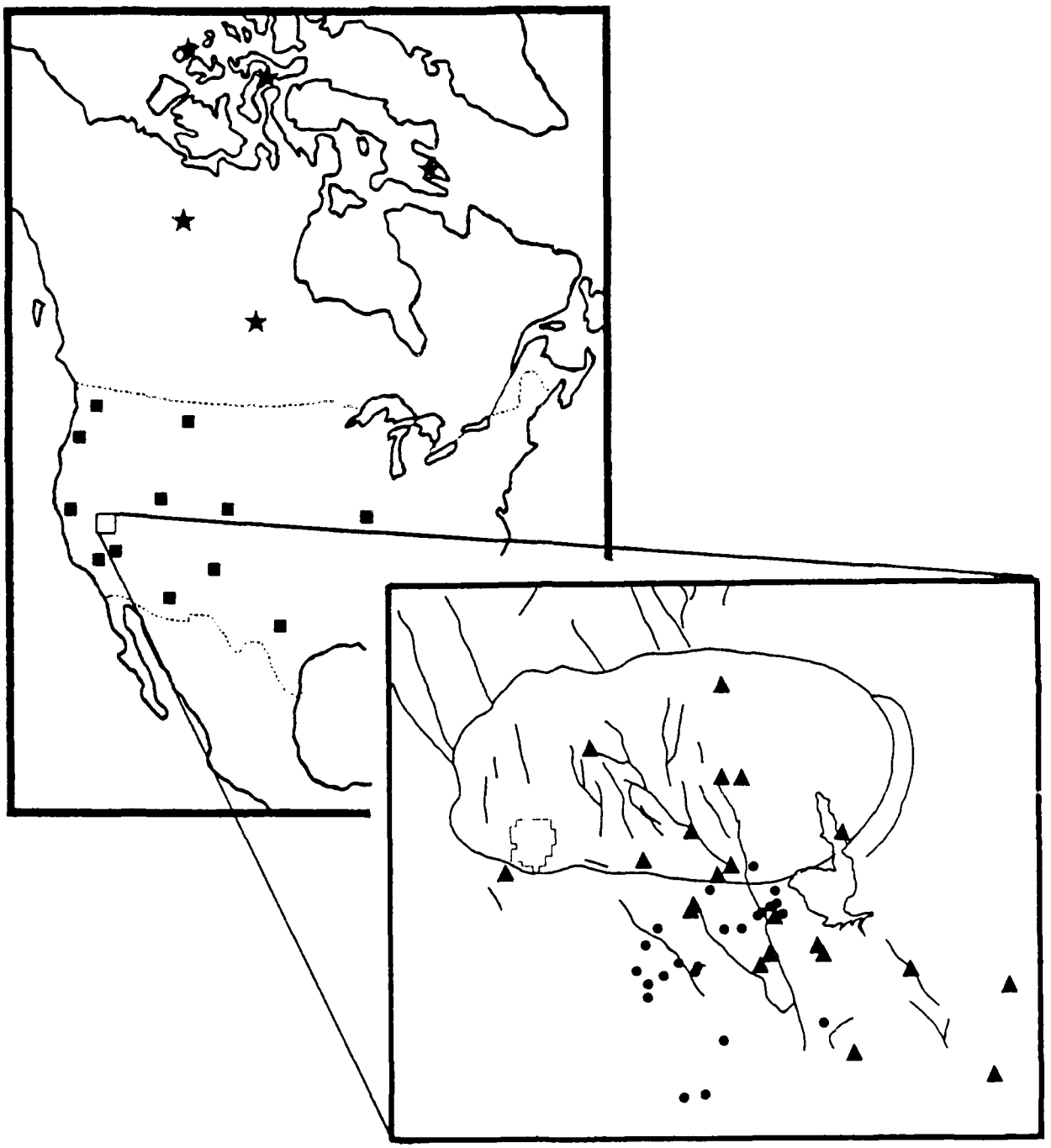

FIGURE 1

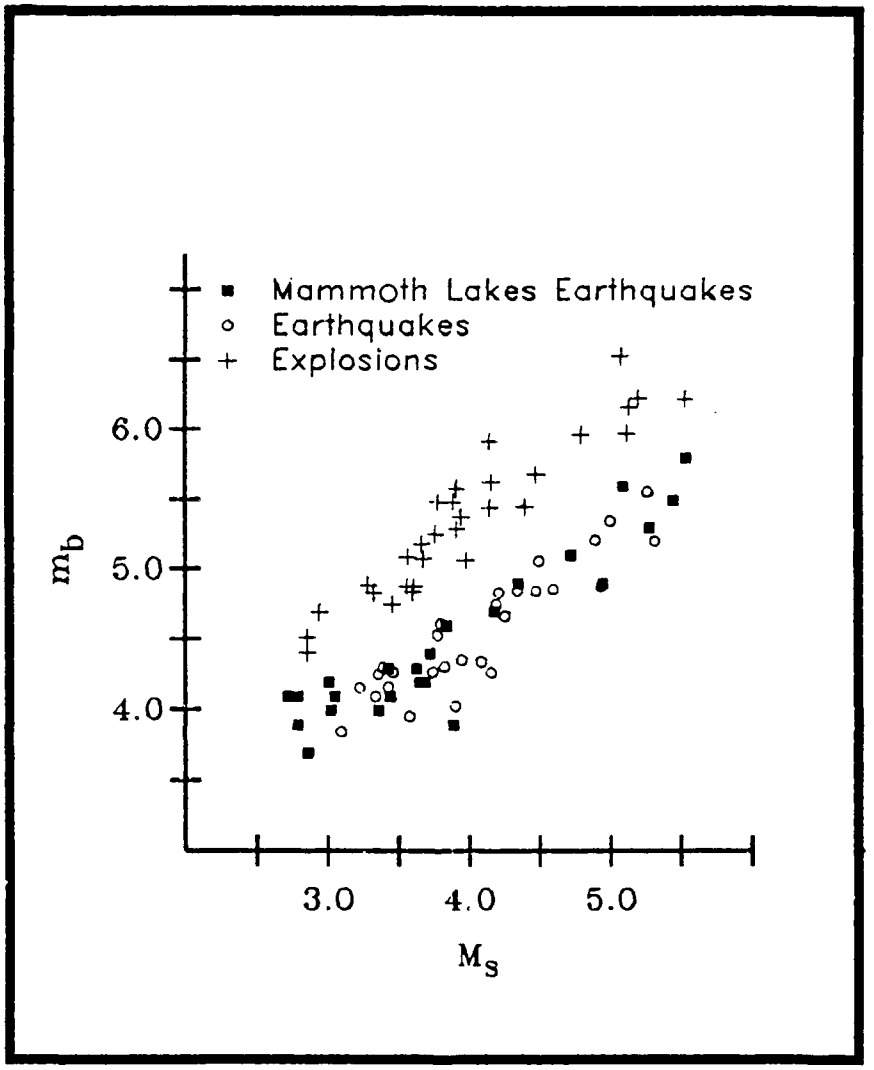
Mammoth Lakes Earthquakes
Earthquakes
Explosions
6.0
5.0
4.0
m_b
3.0
4.0
5.0
M_S

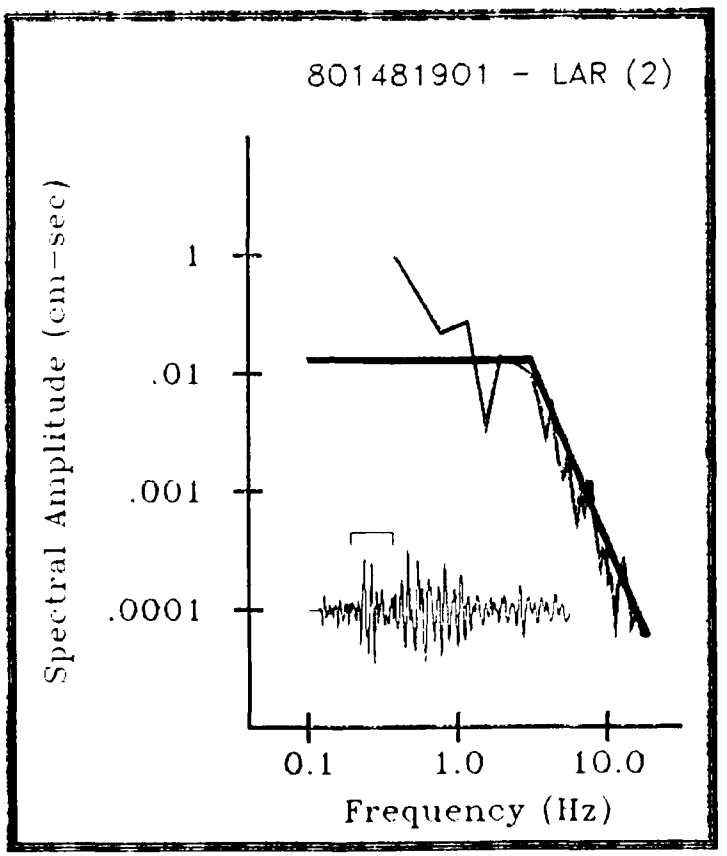
801481901 - LAR (2)
Spectral Amplitude (cm-sec)
1
.01
.001
.0001
0.1
1.0
10.0
Frequency (Hz)

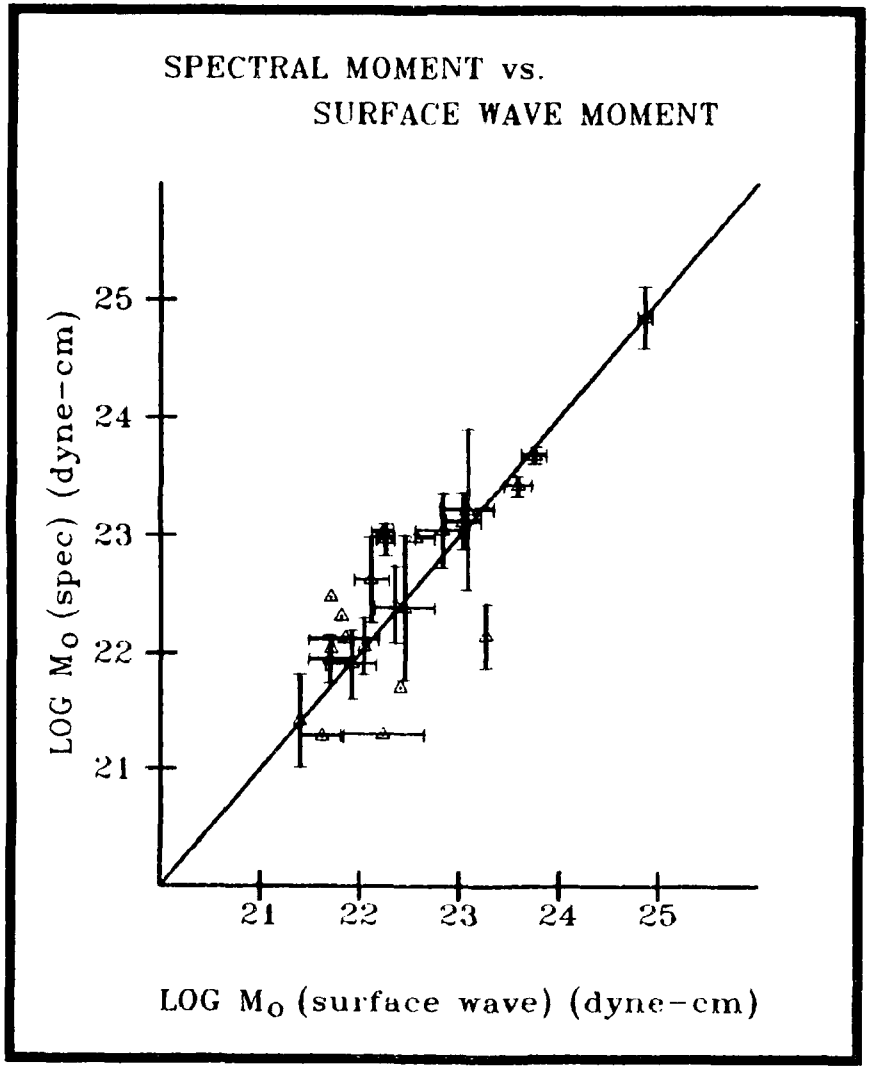
SPECTRAL MOMENT vs.
SURFACE WAVE MOMENT
LOG Mo (spec) (dyne-cm)
25
24
23
22
21
21
22
23
24
25
LOG Mo (surface wave) (dyne-cm)

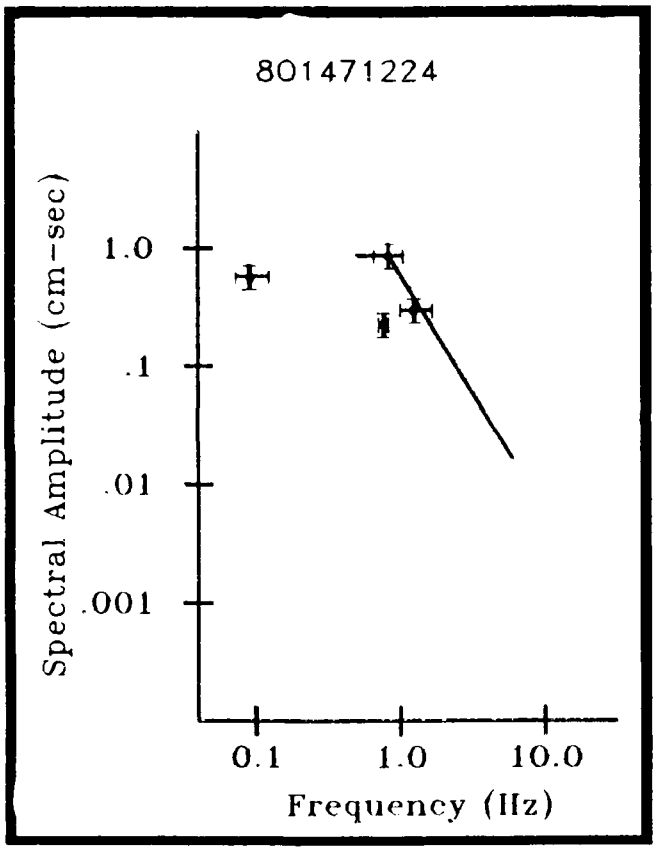
801471224
Spectral Amplitude (cm-sec)
1.0
.1
.01
.001
0.1
1.0
10.0
Frequency (Hz)

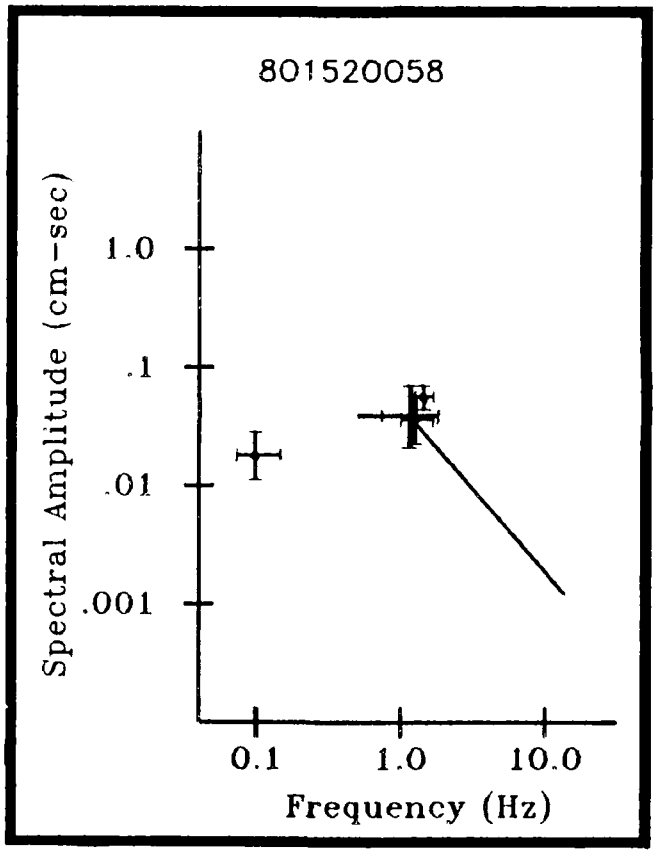
801520058
Spectral Amplitude (cm-sec)
1.0
.1
.01
.001
0.1
1.0
10.0
Frequency (Hz)

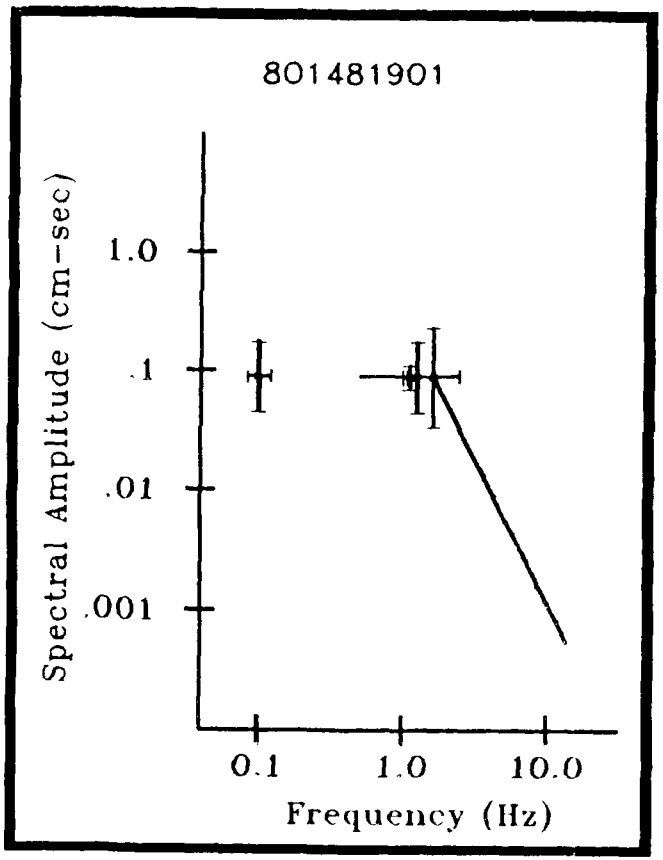
801481901
Spectral Amplitude (cm-sec)
1.0
.1
.01
.001
0.1
1.0
10.0
Frequency (Hz)

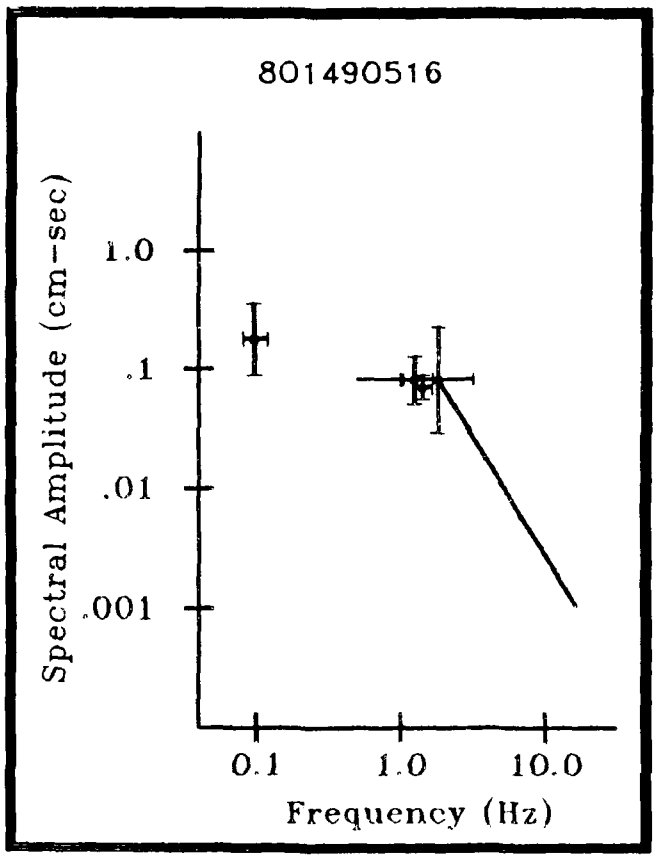
801490516
Spectral Amplitude (cm-sec)
1.0
.1
.01
.001
0.1
1.0
10.0
Frequency (Hz)

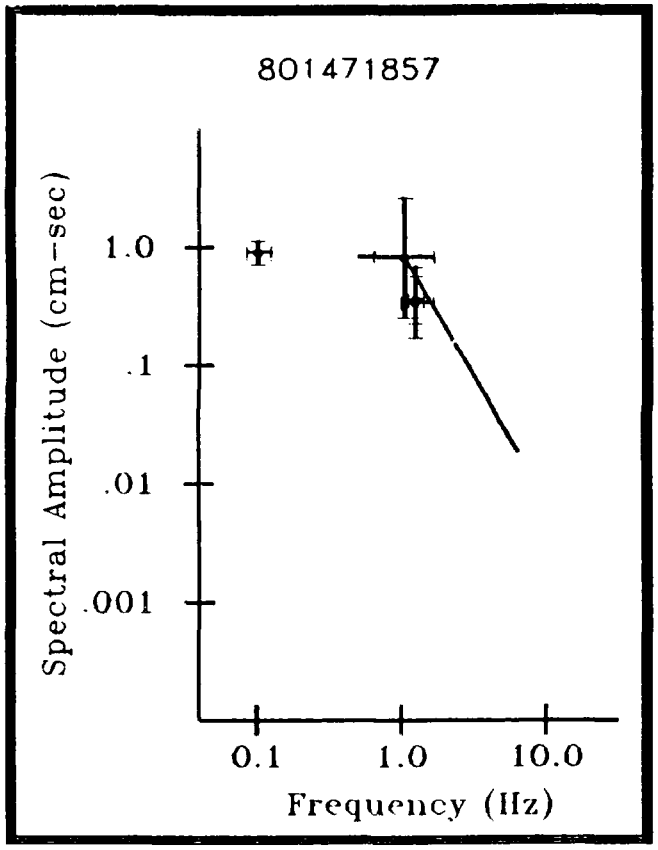
801471857
Spectral Amplitude (cm-sec)
1.0
.1
.01
.001
0.1
1.0
10.0
Frequency (Hz)

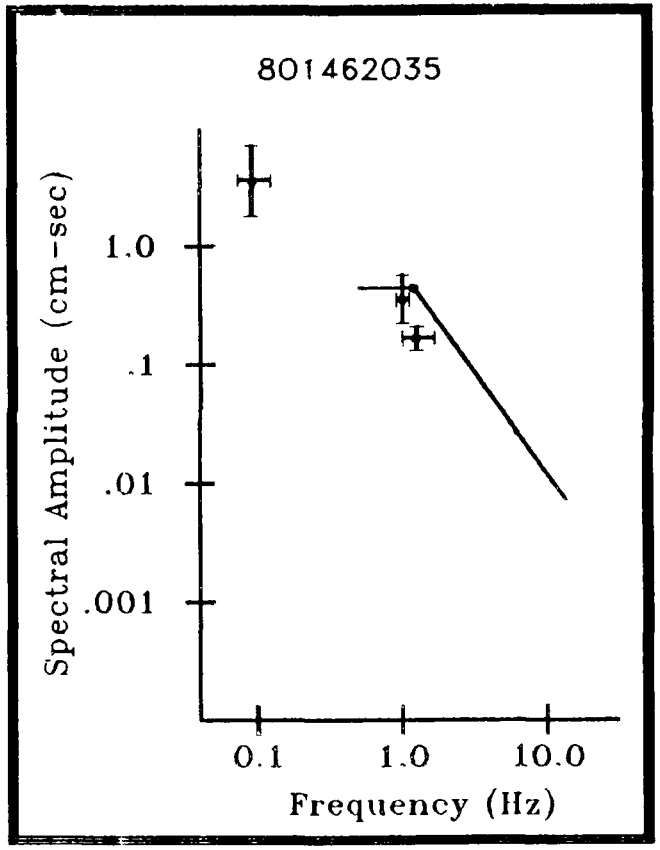
801462035
Spectral Amplitude (cm-sec)
1.0
.1
.01
.001
0.1
1.0
10.0
Frequency (Hz)

THE M_L SCALE IN THE GREAT BASIN AND M_o vs M_L RELATIONSHIPS FOR THE 1980 MAMMOTH LAKES, CALIFORNIA EARTHQUAKE SEQUENCE

David E. Chavez and Keith F Priestley

ABSTRACT

We have converted 471 seismograms from 103 earthquakes in the vicinity of Mammoth Lakes, California into equivalent Wood-Anderson seismograms and estimated local magnitude M_L following the original definition made by Richter. We found that the distance correction terms given by Richter's attenuation curve yield systematically larger M_L estimates for distances less than 20 km. M_L determined at near distances ($\Delta < 10$ km) using Richter's $\log A_o$ values are as much as 1 magnitude unit greater than M_L determined at regional distances ($\Delta > 50$ km) for the same event. This result is similar to those of recent studies utilizing southern California and northern Baja California earthquakes. Seismograms recorded at greater distances in the Great Basin (100 km $< \Delta <$ 300 km) show more attenuation (about 0.3 magnitude units) than that predicted by Richter's curve. We have determined corrections to the attenuation curve which removes the distance dependence observed for our data. We also find a near source local magnitude saturation for events with $M_L \geq 6.0$ similar to earlier studies with California earthquakes and explained as finite source size effects. Using the revised magnitude scale and seismic moments estimated from spectral analysis we found that our data were well fit by the straight line

$$\log M_o = (1.22 \pm 0.04) M_L + (16.98 \pm 0.15)$$

for $1.5 \leq M_L \leq 6.3$. Comparison of our data to predicted M_o versus M_L values suggest a constant stress drop of approximatley 100 bars for events with $M_L < 5.0$ and increasingly greater stress drop for the larger events.

Introduction

Local magnitude, M_L, was defined by Richter (1935) to be

$$M_L = \log A - \log A_o (\Delta)$$

where A is the maximum zero to peak trace amplitude in millimeters recorded

on a standard Wood-Anderson torsion seismograph (static magnification = 2800, natural period = 0.8 sec, and damping factor = 0.8) at an epicentral distance Δ. The $\log A_o(\Delta)$ function removes the distance dependence of the amplitude, incorporating geometrical spreading, change in wave type, scattering, and anelastic attenuation. The nature of these last three will depend on the structure between the source and receiver and in general will vary between regions. Richter emperically determined the shape of the $\log A_o(\Delta)$ curve for southern California and calibrated it so that an event of $M_L = 0$ would have a peak Wood-Anderson trace amplitude of one micron at an epicentral distance of 100 km. Initially the curve was defined for the range $25\,km < \Delta < 600\,km$, however later Gutenburg and Richter (1942) extended it to zero distance using data from low gain torsion seismographs.

The $\log A_o(\Delta)$ values published in Richter (1958, p. 342) have been used in estimating M_L outside of the southern California region for which they were developed. As pointed out in a number of studies, this implies that the attenuation function is the same as in southern California. This will not always be the case, however, and consequently equal numerical M_L values for earthquakes in different regions will not neccesarily imply the same seismic energy release at the source. This is of interest in engineering seismology because M_L (and hence $\log A_o(\Delta)$) plays an important role in the analysis and prediction of strong ground motion.

Few Wood-Anderson attenuation functions have been determined for areas outside of southern California primarily because of the lack of a sufficient number of standard seismographs with which to constrain the curve. The increasing availability of digital seismograms from calibrated stations now offers the possibility of doing so by creating "synthetic" Wood-Anderson seismograms. For example, Bakun (1984a) used such data to develop a $\log A_o(\Delta)$ curve for central California. He found that the original southern California curve was appropriate except for some modification at near distances. Also, three recent studies in the southern California region (Luco, 1982; Jennings and Kamamori, 1983; Munguia and Brune, 1984) have used strong motion and/or digital recordings to determine M_L at near distances. Each of these have found a systematic trend in M_L with distance, indicating that the $\log A_o$ attenuation function used in calculating M_L is not correct close to the epicenter. Moreover, they found that the nature of these variations with distance are a function of recorder site characteristics and the size of the event as well. For instance, all reported that for large events ($M_L \geq 6.0$) local magnitude was underestimated at distances below about 20 km relative to that determined at more distant stations. Munguia and Brune also found that for smaller events ($M_L \leq 5.5$) local magnitude was increasingly overestimated as epicentral distance grew less. In all cases, no modifications to Richter's (1958) curve were found to be necessary beyond 100 km.

In this paper we use events in the vicinity of Mammoth Lakes, California recorded both near the source and at regional distances to develop a $\log A_o(\Delta)$ curve for the Great Basin. We are fortunate in that ray paths from Mammoth Lakes eastward travel exclusively in the Great Basin while paths westward travel through the areas where Richter's (1958) curve was defined or later shown to be applicable. This allows us to directly calibrate our attenuation curve to that for which M_L was originally defined.

For most applications outside of engineering, the seismic moment M_o is often a preferable measure of earthquake size since moment is directly related to specific source properties, namely the fault area and amount of slip. Moreover, M_L will saturate for events sufficiently large that the corner frequency is

below the Wood-Anderson passband while M_o will not. Theoretical source models and the widespread use of digital recordings have made possible routine estimation of M_o for a large range of sizes. Here, we develop a M_o versus M_L relationship for events in the 1980 Mammoth Lakes sequence and compare it to similar relations for other areas.

Data and Analysis

The data analyzed in this study consist of seismograms of earthquakes in the vicinity of Mammoth Lakes, California, primarily events of the 1980 sequence (Urhammer and Ferguson, 1980). The data at distances less than 30 km include velocity and acceleration records obtained by the U. S. Geological Survey (Archuleta, *et al.*, 1982), and strong motion accelerograms from instruments installed by the California Divisions of Mines and Geology (Turpin, 1980) and by the University of Southern California-California Institute of Technology (Moslem, *et al.*, 1983). For distances from 100 to 600 km we have data from broad-band stations operated by the Lawrence Livermore National Laboratory. Similar broad-band instruments installed by the University of Nevada recorded aftershocks of the November 23, 1984 $M_L = 5.7$ earthquake near Bishop, California. We have also used seismograms from the Wood-Anderson seismograph at Dugway, Utah. In all, 471 seismograms for 103 earthquakes in the range $0.8 \leq M_L \leq 6.3$ were studied. Figure 1 is a map showing the source regions, station locations, and travel paths analyzed.

Following Bakun (1978), we have synthesized Wood-Anderson seismograms by transforming the original time series into the frequency domain and deconvolving the original instrument response, thus converting the spectrum to ground displacement. This complex ground displacement spectrum was then convolved with a Wood-Anderson response, and the resulting spectrum transformed back to the time domain to give a "synthethic" Wood-Anderson seismogram, i.e. that which would have been recorded at the site had the original instrument been replaced with a Wood-Anderson torsion seismograph with sufficient dynamic range. Maximum zero-to-peak amplitudes were determined from the Wood-Anderson seismograms, and these values were converted to a $M_L\,(syn)$ using the $\log A_o$ table given in Richter (1958).

In keeping with the original definition of local magnitude, we have used epicentral distance when determining the $\log A_o$ term. Jennings and Kanamori (1983) examined the effect of different measures of distance on estimates of near source M_L and found that epicentral distance was not inappropiate when it was large compared to the fault length. For all but the largest of the events this assumption is valid and since the fault lengths for the large earthquakes are not known, we used epicentral distance in those cases as well.

We used M_L as reported by the Univerisity of California at Berkeley and the California Institute of Technology as a "true" reference magnitude. When both institutions reported a M_L for a given earthquake we used the average as our reference, otherwise we used the single value given (which usually is an average over several stations). Calling the reference magnitude $M_L\,(WA)$, we plotted $M_L\,(syn) - M_L\,(WA)$ versus distance. Deviations from the zero line in these plots indicate differences between the Great Basin $\log A_o(\Delta)$ curve and Richter's (1958) curve with which the reference magnitudes were determined. Positive "residual" magnitudes reflect larger $\log A_o$ values than Richter's while negative residuals are due to smaller $\log A_o$ values.

Determination of $\log A_0(\Delta)$ for the Great Basin

Figure 2a is the $M_L(syn) - M_L(WA)$ versus distance plot for all data with $M_L \geq 6.0$. We observe a near source saturation of M_L for these large events similar to that observed for comprable sized earthquakes in southern California (Luco, 1982; Jennings and Kanamori, 1983) and northern Baja California (Munguia and Brune, 1984). Specifically, we find that for $\Delta \leq 20$ km M_L is consistently underestimated by a few tenths to almost one magnitude unit while at greater distances ($\Delta > 40$ km) we obtain mostly positive residuals.

Munguia and Brune (1984) have postulated a possible mechanism for this observation. They suggest that low M_L for large events recorded at near distances arise from a complex near-source spreading out the waveform in time as a result of the larger source size. They describe an experiment in which they use a small event ($M_L = 4.8$) as an emperical Green's function which is summed over a rectangular fault to determine the seismogram for a larger event at both near and regional distance. They find that at greater epicentral distances ($\Delta > 50$ km) the arrivals from various portions of the fault constructively add to produce larger amplitude arrivals and hence yield a greater Wood-Anderson magnitude. However, at near distances ($\Delta < 20$ km) the arrivals are not in phase, leading to a lower estimate of M_L. This same situation appears to apply for the large events we have studied.

Figure 2b is a plot of the same data as in Figure 2a except that Jennings and Kanamori's (1983) modifications to Richter's (1958) attenuation curve have been applied. This brings our data into agreement with the California Wood-Anderson stations. In both Figures 2a and 2b, the data at the 500 to 600 km range agree reasonably well with the California data. This could lead one to conclude that at those distances the Great Basin attenuation curve matches the southern California curve. However, we feel that our data for smaller events do not support such a conclusion, as we discuss below.

In Figure 3 we plot $M_L(syn) - M_L(WA)$ versus distance for all data with $M_L \leq 5.5$. Although there is considerable scatter, two gross features are obvious. First, at near distances ($\Delta < 15$ km) Richter's $\log A_0$ curve results in an overestimation of M_L relative to the more distant California stations by as much as one magnitude unit. Second, at larger distances ($\Delta > 75$ km) Richter's curve causes the Great Basin estimates of M_L to be about 0.3 magnitude units too low. We shall consider each observation separately.

Figure 4a shows the near source data in greater detail while, for clarity, Figure 4b shows the data for two individual events. The reduction in scatter visible in Figure 4b indicates that much of that in Figure 4a is probably due to variations in source properties between different events. Both plots show a systematic increase in $M_L(syn) - M_L(WA)$ with decreasing distance, ranging from near zero at $12 \leq \Delta \leq 30$ km up to about one at zero distance. These observations are very similar to those made by Munguia and Brune (1984) for comprable sized earthquakes in southern California and northern Baja California. Consequently, we feel that this near source overestimation of M_L is due to the fact that Richter's (1958) attenuation curve is poorly constrained at close distances and not to any physical differences between the western Great Basin and southern California.

We have determined modificatons to the $\log A_0$ curve for $\Delta < 20$ km which remove the observed bias from both our data and that of Munguia and Brune (1984, fig. 4). Figures 4c and 4d show the result of computing M_L with this revised curve. We point out that the sense of this correction for our close-in data is opposite to that given in Jennings and Kanamori (1983) since here we are

dealing with smaller events which do not demonstrate the effect of finite source size. Thus, at near distances two attenuation curves are required in order to compute M_L over a complete magnitude range.

Turning our attention now to the data in the 100 to 600 km distance range (Figure 3a) we note that at all distances except at about 600 km, M_L is on the average underestimated by about 0.3 magnitude units. Those data at 600 km correspond to the station at Dugway, Utah which is located on sediments. All the other stations at regional distances are installed on bedrock, so it is possible that the Dugway "anomaly" is a result of sediment amplification. We conclude from Figure 3a that within the Great Basin there is greater attenuation of seismic energy in the Wood-Anderson passband than in southern California.

This result is not inconsistent with other geophysical studies in the Great Basin, which show that it is a region of active crustal spreading characterized by high heat flow (Sass, *et al.*, 1977) and a low velocity, high attenuation upper mantle (Archambeau, *et al.*, 1969). Patton and Taylor (1984) concluded that the shear wave Q was about 100 in the lower crust and 30 in the upper mantle which is less than the coda Q of 200 Singh and Herrmann (1983) found for California. This is in conflict, however, with Evernden's (1975) study of intensities in the Great Basin which concluded that it has slightly less attenuation than California.

Nevertheless, our data require a systematic increase in attenuation relative to southern California in order to bring our M_L estimates into agreement with those made using the Berkeley and Pasadena Wood-Anderson recordings of the same earthquakes. We have done so, and Figure 3b shows the result of our corrections. In Figure 5 we plot our $\log A_o$ curve for the Great Basin together with Richter's (1958) curve and Jennings and Kanamori's (1983) modification to it. For $\Delta < 15$ km the Great Basin curve rises above Richter's, is the same as his for $15 < \Delta < 35$ km, and then falls below it by a constant factor of 0.3.

All of our work is predicated on the assumption that our reference magnitude (the average of the U. C. Berkeley and Caltech magnitudes) is correct, however this may not be the case. Bakun (1984a) reports on a possible miscalibration of the Berkeley Wood-Anderson seismographs in which it appears that the Berkeley instruments operate at a gain of 2100 rather than 2800 as required by the definition of M_L. If this is the case, then our baseline could be as much as 0.12 magnitude units too high. This shift in the baseline would affect only the details of our conclusions, however. The near source overestimation of M_L observed for the smaller events would be enhanced and although the underestimation found for the same data at regional distances would be reduced, it would still persist. Furthermore, since for most events we include the Caltech magnitude in our average, the effect of the Berkeley miscalibration should be less than 0.12 units.

M_o vs M_L relationships for the 1980 Mammoth Lakes sequence

Using the $\log A_o(\Delta)$ curve developed here for the smaller events and Jennings and Kanamori's (1983) curve for the larger events, we recomputed M_L for 71 earthquakes of the 1980 Mammomth Lakes, California sequence. Figure 6 is a plot of these revised magnitudes versus the seismic moment taken from Archuleta, *et al.* (1982) and Priestley, *et al.* (1985). These moments are based on spectral analysis of the same digital and strong-motion recordings from which the synthetic Wood-Anderson seismograms were derived. Both Archuleta, *et al.* (1982) and Priestley, *et al.* (1985) obtained similar values of seismic

moment when they examined seismograms common to both studies. In addition, Priestley, *et al.* determined the moments of the larger ($M_L \geq 4.0$) events from regional surface wave recordings and found them to be in agreement with those determined from spectral analysis of the local recordings. In the figure, error bars denote the spread in M_L and M_o for multiple recorded events.

Two straight lines fit the data. For events in the magnitude range $3.0 \leq M_L \leq 6.25$, the data are fit by the line

$$\log M_o = (1.22 \pm 0.04) M_L + (16.98 \pm 0.15) \qquad (1)$$

The smaller events ($M_L \leq 1.5$) deviate from this line. For events in the magnitude range $0.8 \leq M_L \leq 3.0$ the moments scatter about the line

$$\log M_o = (0.70 \pm 0.11) M_L + (18.26 \pm 0.24)$$

however it is strongly affected by the four smallest events. There are very few recordings for these four events and it could be easily argued that neither their moments nor their magnitudes are well determined.

The M_o versus M_L relationship given in equation (1) can be compared to that given by Archuleta, *et al.* (1982) which used data primarily in the range $3.0 \leq M_L \leq 5.0$ with only one event above $M_L = 5.0$. Our data, on the other hand, span the range $0.8 \leq M_L \leq 6.3$ with eight events above $M_L = 5.0$. Archuleta, *et al.* (1982) found that the M_o versus M_L relationship for the 40 events for which they had Berkeley M_L determinations was, for the range $2.9 \leq M_L \leq 6.2$,

$$\log M_o = (0.96 \pm 0.06) M_L + (18.14 \pm 0.23)$$

but for the larger events with more reliable M_L estimates ($3.5 \leq M_L \leq 6.2$) it was

$$\log M_o = (1.05 \pm 0.08) M_L + (17.76 \pm 0.33)$$

The greater slope in equation (1) is due to the larger moments which we used for events with $M_L > 5.0$. For example, for the May 27, 1980 event at 14:50, Archuleta, *et al.* (1982) found a seismic moment of 2.33×10^{24} dyne-cm based on two recordings whereas Priestley, *et al.* (1985) obtained a value of 7.24×10^{24} dyne-cm when using nine recordings.

In comparing our data with other regions of California, the slope of our curve is less than the least squares fit Archuleta, *et al.* (1982) made to the data in Thatcher and Hanks (1973), but is essentially identical to the relation found by Bakun and Lindh (1977)

$$\log M_o = (1.21 \pm 0.03) M_L + (17.02 \pm 0.07)$$

for the Oroville, California earthquake sequence. Oroville is located in the western Sierra Nevada in a tectonic environment which is more similar to that of Mammoth Lakes than the southern California region studied by Thatcher and Hanks (1973).

In a recent study of five different source regions (Parkfield, San Juan Bautista, the Sargent fault, Coyote Lake, and the Livermore Valley), Bakun (1984b) detected an inflection in the $\log M_o$ versus M_L plot at about $M_L = 3$. For the events in the range $1.5 \leq M_L \leq 3.5$ he found the relationship to be

$$\log M_o = 1.2 M_L + 17$$

which is essentially the same relationship given in equation (1) based on data in the range $3.0 \leq M_L \leq 6.25$. However, for events in the similar range $3.5 \leq M_L \leq 6.25$ Bakun (1984b) found the relationship to be

$$\log M_o = 1.5 M_L + 16$$

Recently, Hanks and Boore (1984) summarized a number of M_o versus M_L relationships published for central and southern California and compared them with model calculations based on Boore (1983). In Boore (1983), seismograms of hypothetical earthquakes are generated by forcing the amplitude spectrum of band-limited, white Gaussian noise to be that predicted by the Brune (1970, 1971) source model. Boore assumed a constant stress drop (of 100 bars), thus restricting the spectrum scaling law to be a function of seismic moment alone.

Hanks and Boore (1984) computed M_o and M_L from these "seismograms" and found that predicted values of M_o versus M_L fit their data up to about $M_L = 6.0$ at which point their M_L values exceeded those of the model. In Figure 6 we have plotted the same theoretical values as given in Hanks and Boore and find that the predictions agree with our data for small magnitude events (if we neglect the four smallest earthquakes mentioned earlier) and depart from our observations at around $M_L = 5.0$. Hanks and Boore (1984) used teleseismic estimates of seismic moment for the four largest Mammoth Lakes events which are 20 to 30 percent greater than the estimates Priestley *et al.* (1985) obtained through spectral analysis of local recordings of these same events. Had we used the larger moments, the predicted M_o versus M_L values would deviate less from the observations. The fact that Boore's (1983) model (which assumes constant stress drop) and our data do not agree for large M_L implies that stress drop for the Mammoth Lakes events is not constant but rather increases with magnitude. This is in agreement with results from spectral analysis (Archuleta, *et al.* 1982; Priestley, *et al.*, 1985) which indicate that the largest events had stress drops on the order of 1000 bars.

Summary

Comparison of peak Wood-Anderson response measurements in the Great Basin to those in California for the same events indicate that there is a near source M_L saturation for events with $M_L \geq 6.0$. For smaller events ($M_L \leq 5.5$) local magnitude is increasingly overestimated at distances less than about 15 km, probably due to the poor constraint on Richter's (1958) attenuation curve. At larger distances, M_L in the Great Basin is underestimated by approximately 0.3 units, suggesting greater attenuation than in California. We have modified Richter's (1958) attenuation curve so as to remove the above bias for Great Basin seismograms. A revised moment-magnitude relationship for the 1980 Mammoth Lakes earthquakes based on the modified curve is similar to that found for Sierra Nevada earthquakes. The relationship obtained suggests a constant stress drop of 100 bars for smaller Mammoth earthquakes but increasingly larger stress drops for events above $M_L = 5$.

Acknowledgements

We thank J. Anderson, R. Archuleta, H. Patton, W. Richins, and A. Shakal for providing us with the bulk of the data used in this study. W. Peppin assisted in the development of the Wood-Anderson conversion program. This research was funded in part by the Defense Advanced Research Projects Agency of the Department of Defense and monitored by the Air Force Office of Scientific Research under contract F49620-83-C-0012, and by the U. S. Geological Survey under contract 14-08-0001-21863.

References cited

Archambeau, C. B., E. A. Flinn, and D. Lambert (1969). Fine structure of the upper mantle, *J. Geophy. Res.*, *74*, 5825-5865.

Archuleta, R. J., E. C. Cranswick, C. Mueller, and P. Spudich (1982). Source paramters of the 1980 Mammoth Lakes, California, earthquake sequence, *J Geophy. Res.*, *87*, 4595-4607.

Bakun, W. H. (1984a). The M_L scale in central California, *Bull. Seismol. Soc Amer.*, *74*, 1827-1844.

Bakun, W. H. (1984b). Magnitudes and moments of duration, *Bull. Seismol. Soc. Amer.*, *74*, 2335-2356.

Bakun, W. H., S. T. Houck, and W. H. K. Lee (1978). A direct comparison of "synthetic" and actual Wood-Anderson seismographs, *Bull. Seismol Soc. Amer.*, *68*, 1199-1202.

Boore, D. M. (1983). Stochastic simulation of high-frequency ground motions based on seismological models of the radiated spectra, *Bull. Seismol. Soc. Amer.*, *73*, 1865-1902.

Brune, J. N. (1970). Tectonic stress and the spectra of seismic shear waves from earthquakes, *J. Geophy. Res.*, *75*, 4997-5009.

Brune, J. N. (1971). Correction, *J. Geophy. Res.*, *76*, 5002.

Evernden, J. F. (1975). Seismic intensities, "size" of earthquakes and related parameters, *Bull. Seismol. Soc. Amer*, *65*, 1287-1313.

Gutenberg, B., and C. F. Richter (1942). Earthquake magnitude, intensity, energy, and acceleration, *Bull. Seismol. Soc. Amer.*, *32*, 163-191.

Hanks, T. C., and D. M. Boore (1984). Moment-magnitude relations in theory and practice, *J. Geophy. Res.*, *89*, 6229-6235.

Jennings, P. C., and H. Kanamori (1983). Effect of distance on local magnitudes found from strong-motion records, *Bull. Seismol. Soc. Amer.*, *73*, 265-280.

Luco, J. E. (1982). A note on near-field estimates of local magnitude, *Bull. Seismol. Soc. Amer.*, *72*, 941-958.

Moslem, K., A. Amini, B. Kontic, J. Anderson, and T. Heaton (1983). Accelerograms from the Mammoth Lakes, California earthquake sequence of May - July, 1980 recorded on a temporary array, Report No. CE 83-01, University of Southern California.

Munguia, L., and J. N. Brune (1984). Local magnitude and sediment amplification observations from earthquakes in the northern Baja California - southern California region, *Bull. Seismol. Soc. Amer.*, *74*, 107-119.

Patton, H. J., and S. R. Taylor, (1984). Q structure of the Basin and Range from surface waves, *J. Geophy. Res.*, *89*, 6929-6940.

Priestley, K. F., J. N. Brune, and J. G. Anderson, (1985). Surface wave excitation and source mechanisms of the Mammoth Lakes earthquake sequence, *J. Geophy. Res.*, in press.

Richter, C. F. (1935). An instrumental earthquake magnitude scale, *Bull Seismol. Soc. Amer., 25*, 1-32.

Richter, C. F. (1958). *Elementary Seismology*, W. H. Freeman and Co., San Francisco, California, 758 pp.

Sass, J. H., W. H. Diment, A. H. Lachenbruch, B. V. Marshall, R. J. Munroe, T. H. Moses, and T. C. Urban (1976). A new heat flow map of the conterminous United States, *U. S. Geological Survey Open File Report, 76*.

Singh, S., and R. B. Herrmann (1983). Regionalization of crustal coda Q in the continental United States, *J. Geophy. Res., 88*, 527-538

Thatcher, W., and T. C. Hanks (1973). Source parameters of southern California earthquakes, *J. Geophy. Res., 78*, 8547-8576.

Turpen, C. D. (1980). Strong-motion records from the Mammoth Lakes earthquakes of May 1980, *Calif. Div. Mines Geol. Preliminary Report 27*.

Urhammer, R. A., and R. W. Ferguson (1980). The 1980 Mammoth Lakes earthquake sequence, *Spec. Rep. Calif. Div. Mines Geol., 150*, 131-136.

Seismological Laboratory
Mackay School of Mines
University of Nevada, Reno, NV 89557

Figure captions

Figure 1. Map of the western United States showing the Mammoth Lakes, California source region (enlargement, epicenters plotted as dots), seismic stations, and ray paths for the data used in this study. The heavy line delineates the border of the Basin and Range. The triangles indicate seismic stations used to determine the Great Basin attenuation curve, the two soild squares give the locations of Berkeley and Pasadena, California.

Figure 2. $M_L\,(syn) - M_L\,(WA)$ versus distance for all events with $M_L\,(WA) \geq 6.0$. *a*) $M_L\,(syn)$ computed using Richter's (1958) $\log A_o$ values. *b*) $M_L\,(syn)$ computed using Jennings and Kanamori's (1983) modifications to Richter's values.

Figure 3 $M_L\,(syn) - M_L\,(WA)$ versus distance for all events with $M_L\,(WA) \leq 5.5$. *a*) $M_L\,(syn)$ computed using Richter's (1958) $\log A_o$ values. *b*) $M_L\,(syn)$ computed using the Great Basin $\log A_o$ curve developed in this study.

Figure 4. *a*) The same data as in Figure 3a with epicentral distance under 30 km. *b*) Two individual events from the data set shown in Figure 4a. Event dates and origin time are given in the upper right corner. *c* and *d*) The same data as in (*a*) and (*b*) except with $M_L\,(syn)$ computed using the Great Basin $\log A_o$ curve.

Figure 5. Comparison of the $\log A_o$ curve obtained for the Great Basin with Richter's (1958) southern California curve and Jennings and Kanamori's (1983) modification to it.

Figure 6. Log M_o versus M_L for earthquakes in the 1980 Mammoth Lakes, California sequence. Stars indicate theoretical values given in Hanks and Boore (1984) assuming a constant stress drop of 100 bars.

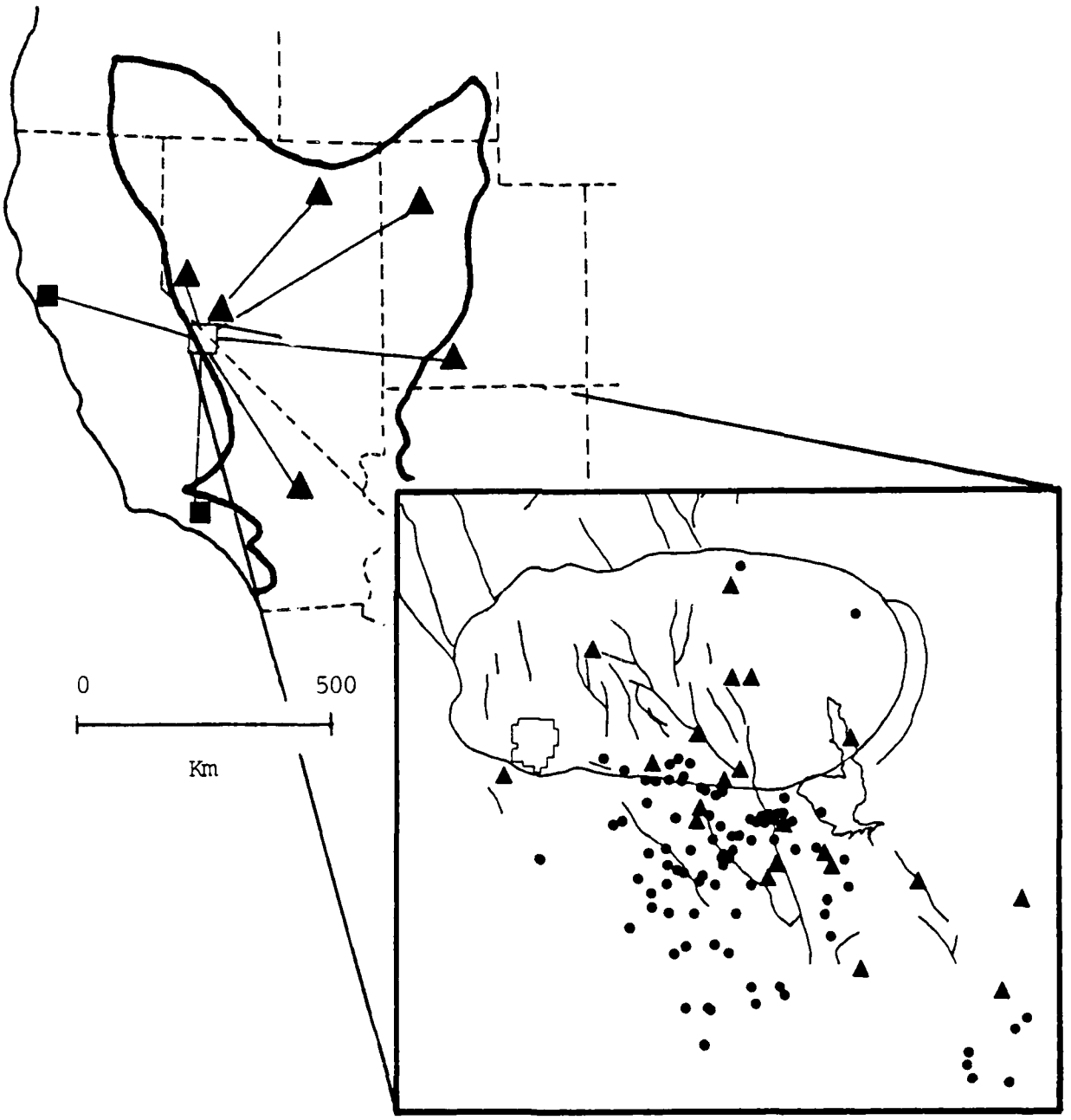

FIGURE 1

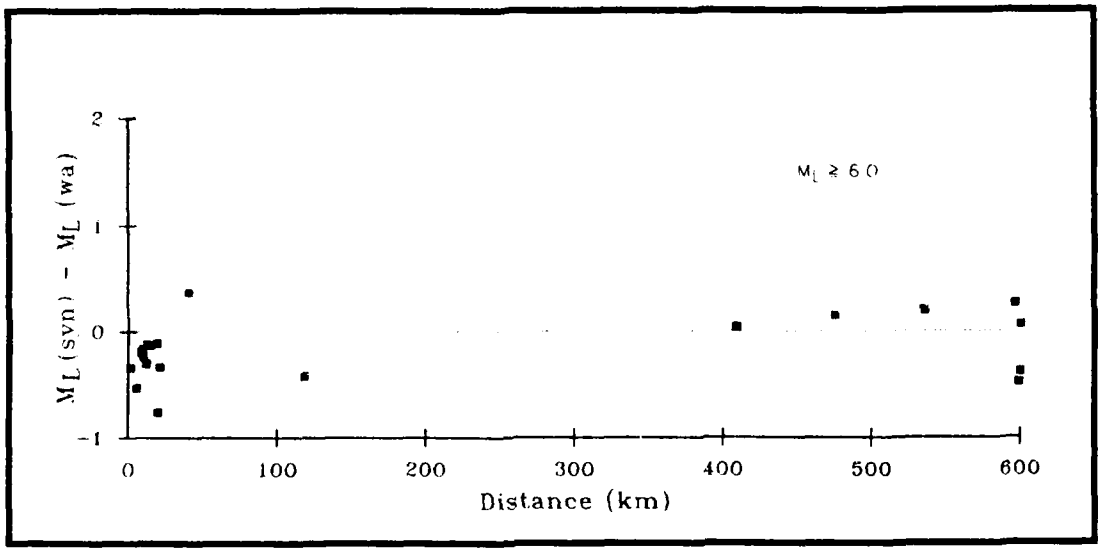
M_L (syn) – M_L (wa)
2
1
0
–1
$M_L \geq 6.0$
0
100
200
300
400
500
600
Distance (km)

(a)

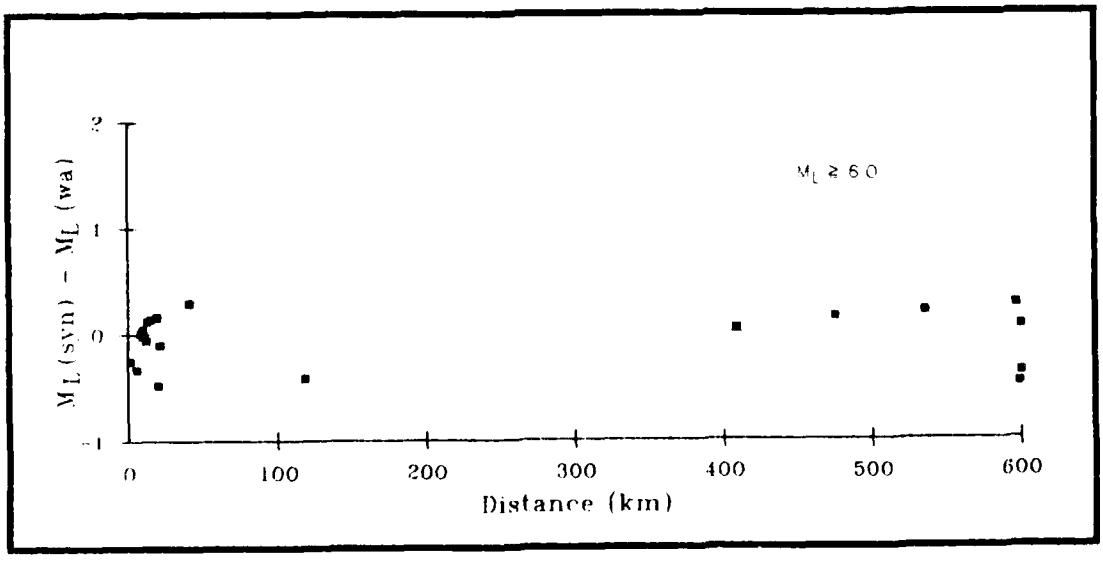
M_L (syn) – M_L (wa)
2
1
0
–1
$M_L \geq 6.0$
0
100
200
300
400
500
600
Distance (km)

(b)

FIGUR E 2

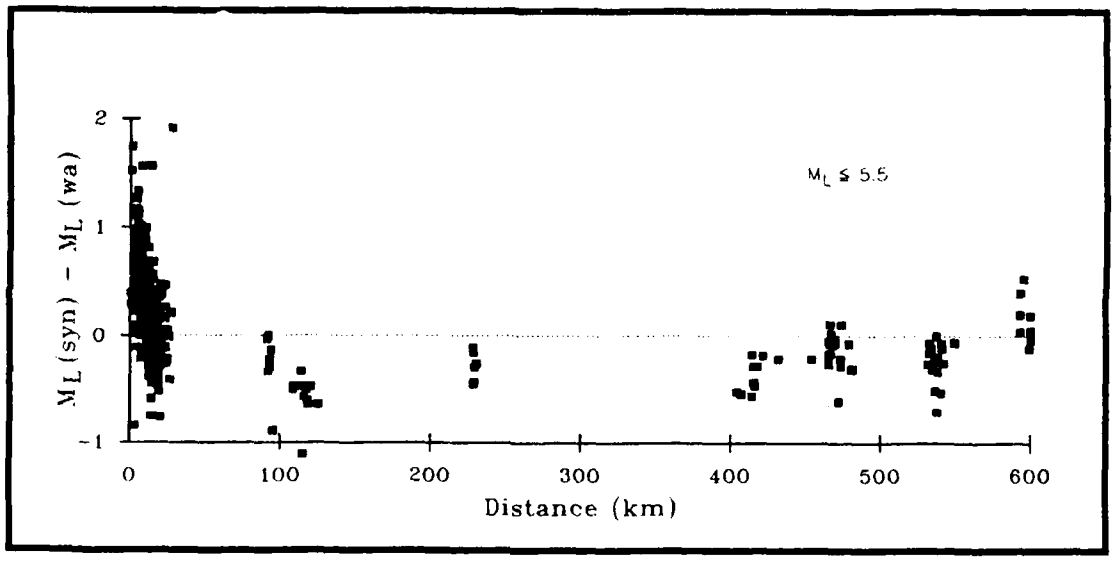
$M_L \leq 5.5$
M_L (syn) – M_L (wa)
2
1
0
-1
0
100
200
300
400
500
600
Distance (km)

(a)

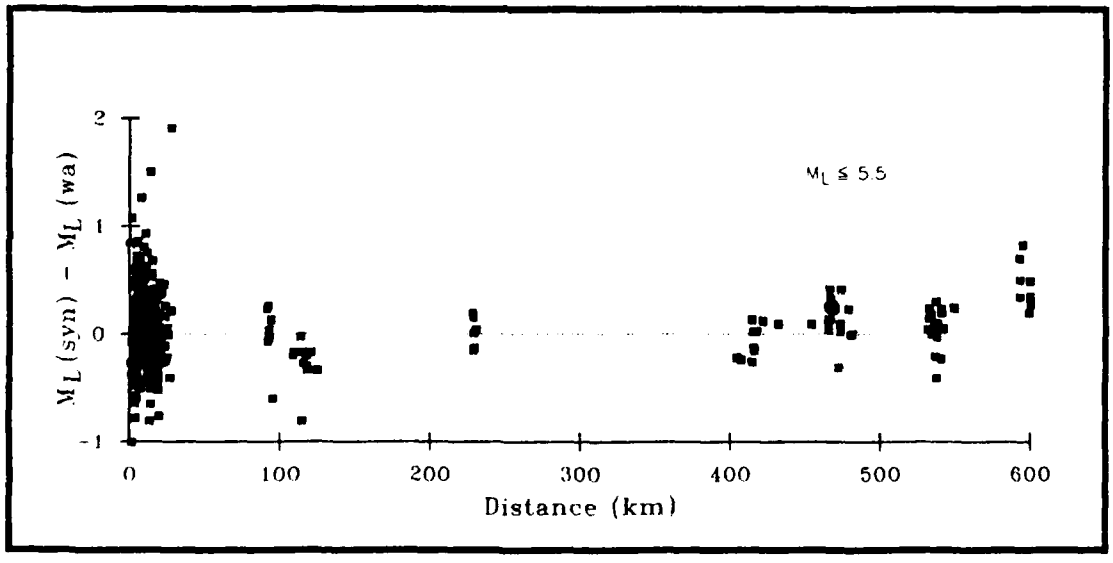
$M_L \leq 5.5$
M_L (syn) – M_L (wa)
2
1
0
-1
0
100
200
300
400
500
600
Distance (km)

(b)

FIGURE 3

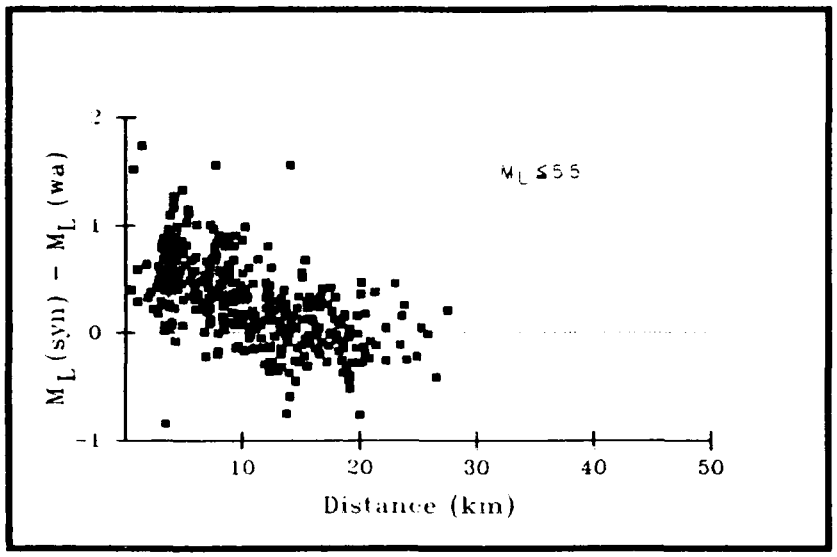

(a)

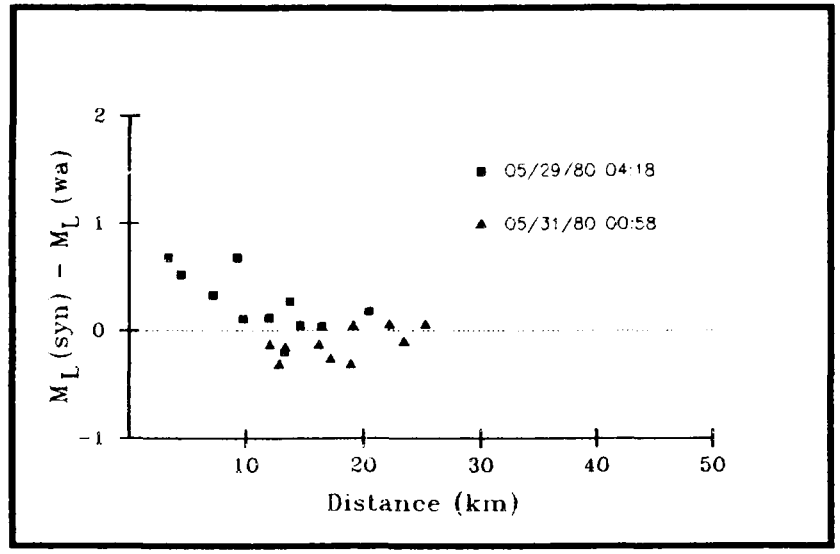

(b)

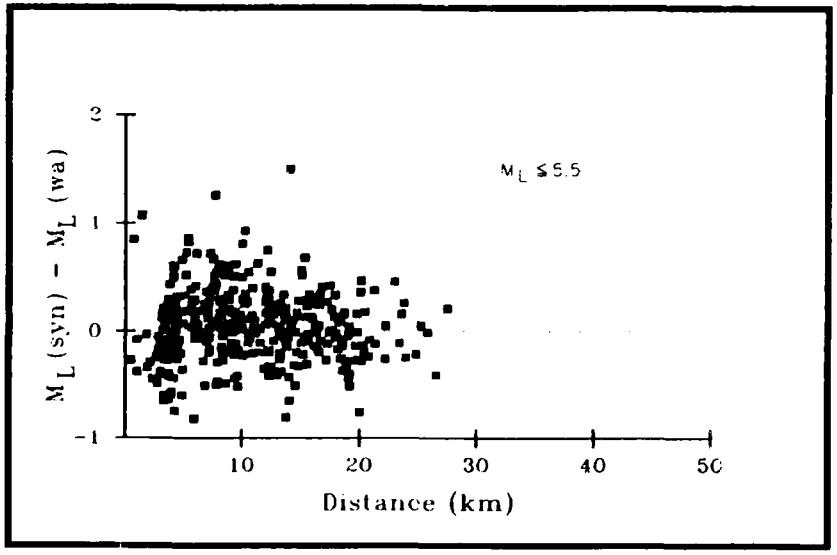

(c)

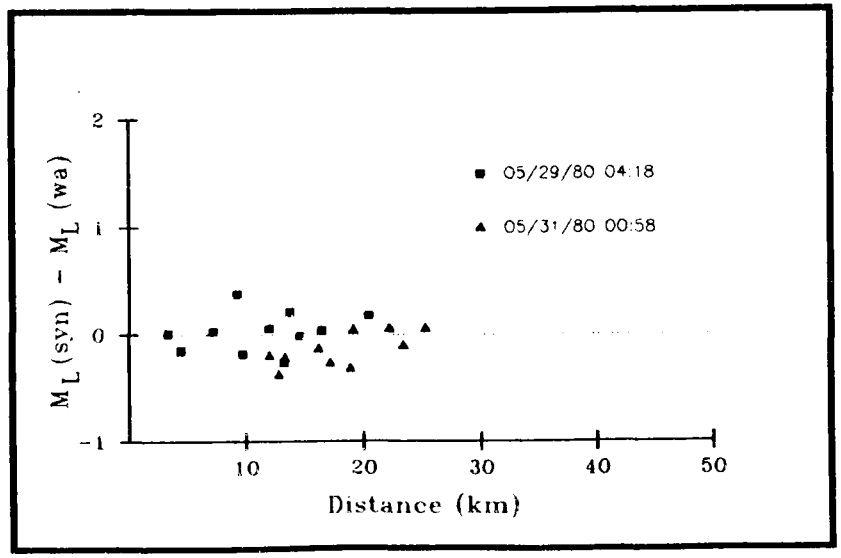

(d)

FIGURE 4

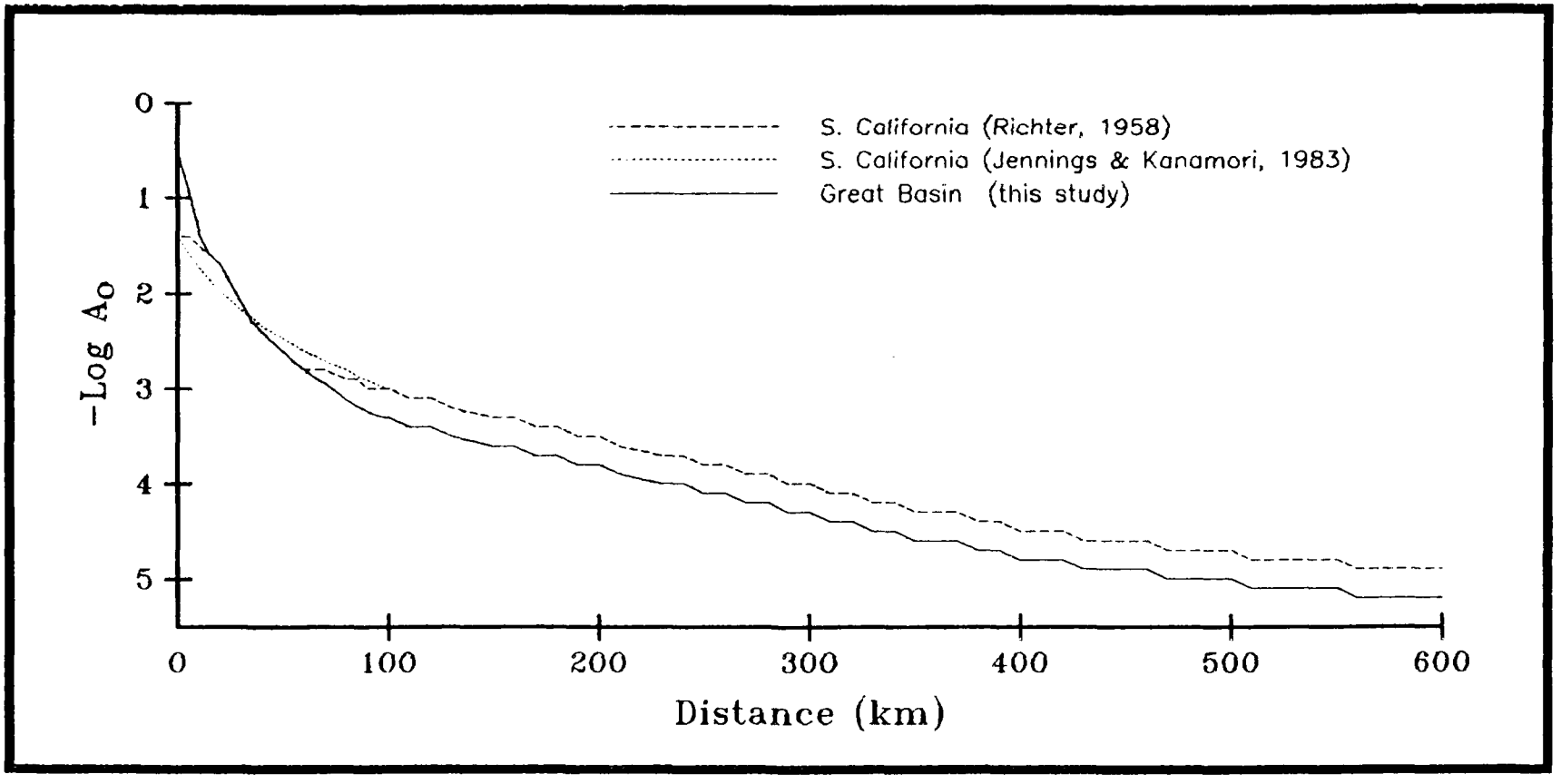
S. California (Richter, 1958)
S. California (Jennings & Kanamori, 1983)
Great Basin (this study)
-Log A_0
0
1
2
3
4
5
0
100
200
300
400
500
600
Distance (km)

FIGURE 5

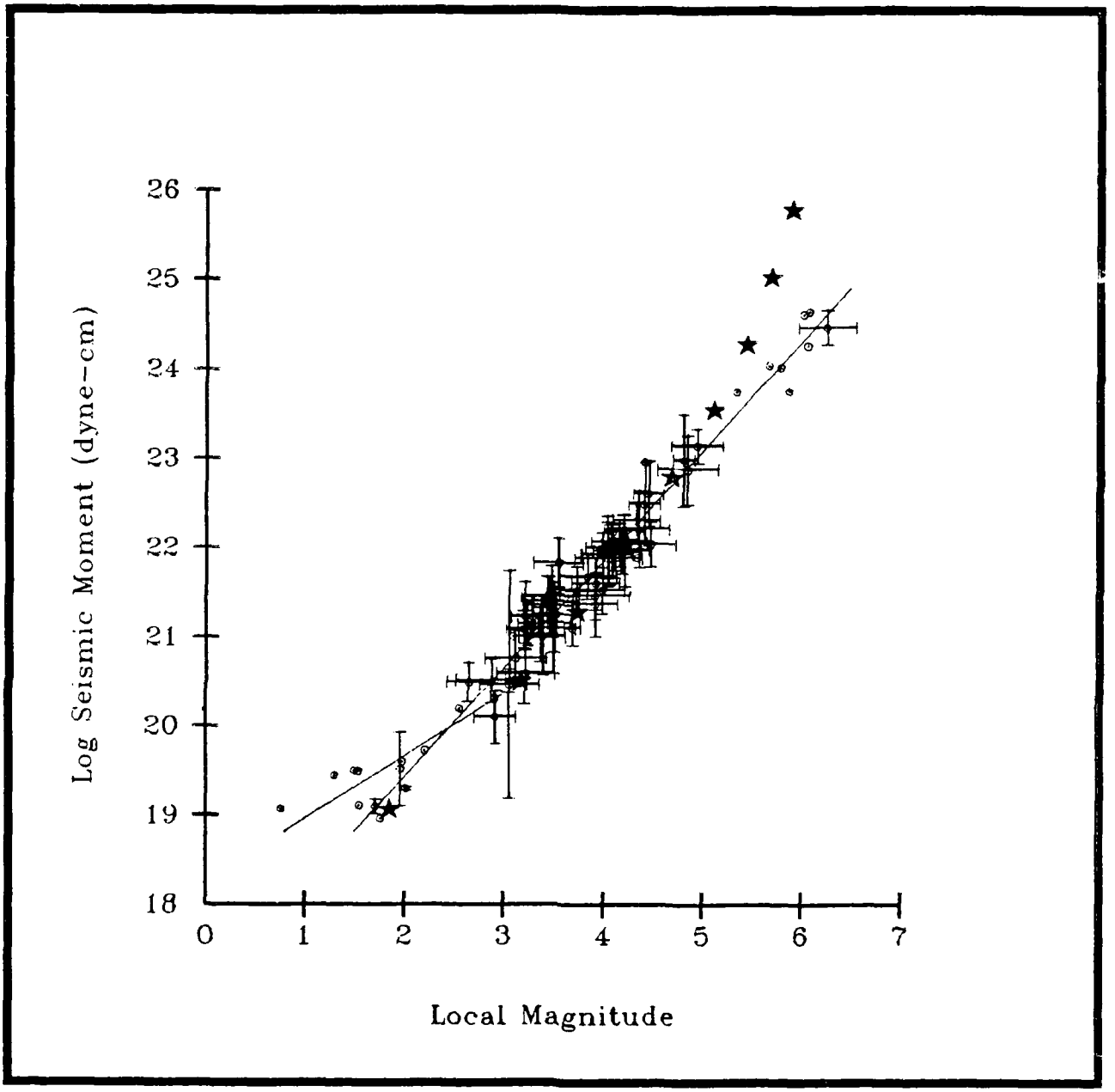
Log Seismic Moment (dyne-cm)
26
25
24
23
22
21
20
19
18
0
1
2
3
4
5
6
7
Local Magnitude

FIGURE 6